Model-Based First-Order Policy Gradient for Contact Dynamics

Shenao Zhang [1] **Wanxin Jin** [2] **Zhaoran Wang** [3]

Abstract

In model-based reinforcement learning (RL), the learned models are typically smooth approximators of the environment dynamics. This is problematic in robotic systems that experience hard contact and have non-smooth or even discontinuous local behaviors. Despite the large amount of data needed to fit these behaviors, the inaccurate model gradient can lead to poor performance when applying First-Order Policy Gradient (FOPG). Therefore, we study the physics-guided model built upon the complementarity problem underlying the contact events. Unfortunately, our theory shows that the complementarity-based model tends to be stiff, and the stiffness causes the FOPG gradient variance to explode, leading to slow convergence and optimization difficulties. For this reason, we define a class of softened complementarity models that correspond to the barrier-smoothed objectives. In this work, we propose to mitigate the large FOPG variance issue using *Analytic Barrier Smoothing*, and control the gradient bias with the *contact-aware* smoothing parameter. In simplified settings, we prove that systems with contact-aware analytic smoothing are the best linear approximators of the exact unsmoothed dynamics, a result obtained by establishing the equivalence between analytic smoothing and randomized smoothing. Based on this result, we provide the gradient bias upper bound of the proposed method. Experimental results also support our theory and method.

1 Introduction

Model-Based Reinforcement Learning (MBRL) has achieved great success in sequential decision-making applications such as board and video games (Schrittwieser et al., 2020; Kaiser et al., 2019). First-Order Policy Gradient (FOPG) by backpropagating through the computational path of cumulative rewards, is the most straightforward method in differentiable simulation (Xu et al., 2022; Freeman et al., 2021) and has shown the potential for general control tasks in model-based settings (Clavera et al., 2020; Li et al., 2021; Amos et al., 2021). However, physical systems, e.g. robotic locomotion and manipulation, have stiff dynamics with extreme curvatures (Parmar et al., 2021; Anitescu & Potra, 2002) due to geometrical constraints and contact events. Most modern MBRL algorithms that fit the dynamics with universal function approximators, such as neural networks (Nagabandi et al., 2018; Chua et al., 2018), tend to select the smoothest interpolators as the simplest explanation of the environment transitions (Belkin et al., 2019; Pfrommer et al., 2021). As a result, the black-box models typically require a large amount of data to learn the contact behaviors while still suffering from inaccurate first-order gradient estimation in long-horizon problems (Hochlehnert et al., 2021).

In this work, we study the physics-guided model built upon the complementarity problem that underlies hard-contact simulations (Geilinger et al., 2020; Howell et al., 2022; Werling et al., 2021). The complementarity problem, from which the impact and frictional contact forces are solved using *Interior-Point Method* (IPM), ensures non-penetration and maximum dissipation. Although the contact dynamics can be well approximated by learning the physical parameters in the complementarity-based model, we show that its stiffness leads to optimization difficulties when performing FOPG. Specifically, we first establish the convergence of model-based FOPG that depends on the gradient variance and bias. Then we prove that the upper bound of the gradient variance has polynomial dependencies on the Lipschitz continuity of the model, where the degrees are linear in the task horizon. When the model is stiff, long chains of nonlinear mappings lead to chaotic (Bollt, 2000) optimization procedure and slow convergence, a phenomenon that is also observed in experiments (Parmas et al., 2018; Metz et al., 2021).

To alleviate the above issue, we define a class of μ-softened *Linear Complementarity Systems* (LCS) with the central-path parameter μ. We prove that the Lipschitz upper bound of the μ-softened LCS scales inversely with μ. Therefore, a natural method to avoid the large gradient variance is to differentiate through the softened complementarity system by setting a stopping criteria in the IPM solver. Since the

[*]Equal contribution [1]Georgia Institute of Technology, Atlanta, GA, USA [2]University of Pennsylvania, Philadelphia, PA, USA [3]Northwestern University, Evanston, IL, USA.

softened LCS can be shown to be the optimality condition of a barrier-smoothed objective, we call this vanilla method *Analytic Barrier Smoothing*. However, simply applying analytic smoothing everywhere can cause unrealistic simulation and a large gradient bias.

To best trade-off between the gradient variance and bias, we propose to use a *contact-aware* central-path parameter that decreases with the minimum distance-to-obstacle of the inactive impact contacts. Intuitively, since the root of stiffness is the sudden change of the impact contact force, smoothing is only needed locally near the impact contact, while the gradients are globally accurate by solving the exact complementarity problem elsewhere. Built upon the equivalence between the analytic barrier smoothing and randomized smoothing (Suh et al., 2022b;a), we prove that the proposed method is the best linear approximation of the exact LCS in frictionless single-contact settings. Based on this result, the gradient bias of contact-aware analytic smoothing can be upper bounded. We also provide experimental results to support our theorem and method.

2 Background

2.1 Reinforcement Learning

Consider learning to optimize a finite H-horizon Markov Decision Process (MDP) over repeated episodes of interaction. Denote the state space and action space as $\mathcal{X}$ and $\mathcal{U}$, respectively. When taking action $u \in \mathcal{U}$ at state $x \in \mathcal{X}$, the agent receives reward $r(x, u)$ and the MDP transitions to a new state according to probability $x' \sim f^*(\cdot \,|\, x, u)$.

We are interested in controlling the system by finding a policy π_θ that maximizes the expected cumulative reward. Denote by ζ the initial state distribution. The objective is

$$\mathcal{J}(\pi) = \mathbb{E}_{x_0 \sim \zeta}\big[V_0^\pi(x_0)\big] = \mathbb{E}_{p_\pi(\alpha)}\left[\sum_{t=0}^{H-1} r(x_t, u_t)\right],$$

where V_0^π is the state value at the initial timestep, and $p_\pi(\alpha)$ is the distribution over rollouts $\alpha := ((x_0, u_0), \cdots, (x_{H-1}, u_{H-1}))$ when executing π, formally, $x_0 \sim \zeta(\cdot)$, $u_i \sim \pi(\cdot \,|\, s_i)$, and $x_{i+1} \sim f^*(\cdot \,|\, x_i, u_i)$.

2.2 Stochastic Gradient Estimation

The general underlying problem of policy gradient, i.e., computing the gradient of a probabilistic objective with respect to the parameters of the sampling distribution, takes the form $\nabla_\theta \mathbb{E}_{p(z;\theta)}[y(z)]$. In RL, we view $p(z;\theta)$ as the trajectory distribution conditioned on policy parameter θ, and $y(z)$ as the cumulative reward. In the sequel, we introduce two commonly used gradient estimators in RL.

Zeroth-Order (Likelihood Ratio) Gradient. By leveraging the *score function*, zeroth-order gradient estimators only require samples of the function values. Specifically, since the score function satisfies $\nabla_\theta \log p(z;\theta) = \nabla_\theta p(z;\theta)/p(z;\theta)$, the zeroth-order gradient has the form:

$$\nabla_\theta \mathbb{E}_{p(z;\theta)}\big[y(x)\big] = \mathbb{E}_{p(z;\theta)}\big[y(z)\nabla_\theta \log p(z;\theta)\big]. \quad (2.1)$$

First-Order (Reparameterization) Gradient. First-order gradient benefits from the structural characteristics of the objective, i.e., how the overall objective is affected by the operations applied to the sources of randomness as they pass through the measure and into the cost function (Mohamed et al., 2020). From the simulation property of continuous distribution, we have the following equivalence between direct and indirect ways of drawing samples:

$$\widehat{z} \sim p(z;\theta) \;\equiv\; \widehat{z} = g(\epsilon;\theta), \quad \epsilon \sim p. \quad (2.2)$$

Derived from the *law of the unconscious statistician* (LOTUS) (Grimmett & Stirzaker, 2020), i.e., $\mathbb{E}_{p(x;\theta)}[y(z)] = \mathbb{E}_{p(\epsilon)}[y(g(\epsilon;\theta))]$, the first-order gradient takes the form:

$$\nabla_\theta \mathbb{E}_{p(z;\theta)}\big[y(z)\big] = \mathbb{E}_{p(\epsilon)}\Big[\nabla_\theta y\big(g(\epsilon;\theta)\big)\Big].$$

2.3 Bundled Gradient via Randomized Smoothing

For non-smooth functions with extreme curvatures, such as objectives for contact dynamics, the gradient may be subject to large jumps. The first-order bundled gradient is proposed by (Suh et al., 2022b;a; Pang et al., 2022) to solve this issue. Consider a deterministic objective $y(x)$. Differentiating through the randomized smoothed objective $\overline{y}(x) := \mathbb{E}_{w\sim\rho(w)}[y(x+w)]$ gives the bundled gradient

$$\nabla \overline{y}(x) = \mathbb{E}_{w\sim\rho(w)}[\nabla y(x+w)].$$

2.4 Rigid-Body Dynamics

We consider a standard approach for modeling robotic systems — the framework of rigid-body systems with contacts. According to the Newton's laws, the continuous-time equation of motion is

$$\mathcal{M}(q)\mathrm{d}v = \big(n(q,v) + u\big)\mathrm{d}t + J(q)^\top \lambda,$$

where we let q denote the generalized coordinates, v the generalized velocities, $u \in \mathbb{R}^{n_u}$ the applied control force, $\mathcal{M}(q)$ the generalized inertia matrix, $n(q,v)$ the passive forces (e.g., Coriolis, centrifugal, and gravity), and $J(q)$ the Jacobian of the active contacts. Here, we define $\lambda := (\gamma^{(1)}, \beta^{(1)}, \cdots, \gamma^{(c)}, \beta^{(c)}) \in \mathbb{R}^{n_\lambda}$ as the (unknown) contact space force, where γ and β are the normal *impact* forces and *frictional* forces, respectively, and c denotes the number of contact points. The state x usually contains q and v.

Using Euler approximation and multiplying by $\mathcal{M}_t^{-1}$, the discrete-time dynamics can be modeled in contact space by

$$\begin{aligned} v_{t+1} &= v_t + \mathcal{M}_t^{-1}(n_t + u_t)h + \mathcal{M}_t^{-1} J_t^\top \lambda_t, \\ q_{t+1} &= q_t + h v_{t+1} \end{aligned} \quad (2.3)$$

where h is the discretization step size and t is the timestep.

The frictional and impact contact forces are constrained by the system's configuration. Specifically, the impact problem is encoded with the following constraints:

$$\gamma_{t+1} \circ \phi(q_{t+1}) = \vec{0}, \qquad \gamma_{t+1}, \phi(q_{t+1}) \geq \vec{0}, \tag{2.4}$$

where $\circ$ is the element-wise (Hadamard) product, $\phi(q_{t+1}) = \phi(x_t, u_t)$ is the signed distance from the contact points to obstacles, $\vec{0}$ is the zero vector, and the equality, inequality are also element-wise. The intuition behind (2.4) is that the magnitude of the normal impact forces must be non-negative and can only be non-zero to maintain non-negative gaps (non-penetration) when there is a contact.

Moreover, the Coulomb friction can be modeled using the maximum-dissipation principle and a linearized friction cone, which has the following set of constraints:

$$\begin{aligned} &\beta_{t+1} \circ \xi_{t+1} = \vec{0}, \qquad \beta_{t+1}, \xi_{t+1} \geq \vec{0}, \\ &B(q_{t+1}) v_{t+1} + \omega_{t+1} \vec{1} - \xi_{t+1} = \vec{0}, \\ &\omega_{t+1} \cdot (\alpha_f \gamma_{t+1} - \beta_{t+1}) = \vec{0}, \end{aligned} \tag{2.5}$$

where $\alpha_f \geq 0$ is the friction coefficient, matrix B maps from the generalized coordinate velocity to tangential velocity in the contact frame, and ω_{t+1}, ξ_{t+1} are dual variables associated with the linearized friction cone and nonnegative constraint, respectively.

3 Complementarity-Based Contact Models

3.1 Softened Linear Complementarity Systems

The dynamic (2.3) describes a hybrid system where different modes are controlled by the contact force λ under the nonlinear complementarity problem (2.4) and (2.5). To simplify our analysis, in the following sections, we study the *Linear Complementarity Systems* (LCS), which effectively capture the local behaviors of the state transitions and are widespread in robotics research (Aydinoglu et al., 2021; Tassa & Todorov, 2010; Drumwright & Shell, 2012).

We first define a class of softened linear complementarity systems f_μ as the approximations of the exact LCS $f_{\mu=0}$.

Definition 3.1 (Softened LCS)**.** A model $x_{t+1} = f_\mu(x_t, u_t)$ is a softened LCS if the evolution of state $x \in \mathbb{R}^{d_x}$ is governed by a linear dynamics and a μ-complementarity problem (the last two lines of (3.1)):

$$\begin{aligned} &x_{t+1} = Ax_t + Bu_t + C\lambda_t + c, \\ &\lambda_t \circ (Dx_t + Eu_t + F\lambda_t + d) = \mu \vec{1}, \\ &\lambda_t \geq \vec{0}, \quad Dx_t + Eu_t + F\lambda_t + d \geq \vec{0}, \end{aligned} \tag{3.1}$$

where $A \in \mathbb{R}^{d_x \times d_x}, B \in \mathbb{R}^{d_x \times d_u}, C \in \mathbb{R}^{d_x \times d_\lambda}, D \in \mathbb{R}^{d_\lambda \times d_x}, E \in \mathbb{R}^{d_\lambda \times d_u}, F \in \mathbb{R}^{d_\lambda \times d_\lambda}$, and $\mu \geq 0$. Denote the solver of the μ-complementarity problem as S_μ, which returns the solution $\lambda_t = S_\mu(Dx_t + Eu_t + d) \in \mathbb{R}^{d_\lambda}$.

In simulation, $\mu = 0$ corresponds to the exact *Linear Complementarity Problem* (LCP) and the LCS $f_{\mu=0}$ resembles the reality. Obviously, solving the contact space force λ_t is our primary goal, since x_{t+1} is readily obtained from the dynamics once λ_t is available. Next, we introduce the assumption and method for solving the exact LCP.

Assumption 3.2 (P-Matrix)**.** Assume F in the LCS (3.1) is a P-matrix, defined as a matrix whose principal minors are all positive, i.e., the determinants of its principal submatrices $\det(F_{\alpha\alpha}) > 0$, $\forall \alpha \subseteq \{1, \cdots, d_\lambda\}$.

Assumption 3.2 guarantees that the solution λ_t exists and is unique, which is commonly assumed in contact dynamics problems (Aydinoglu et al., 2020; Jin et al., 2022).

3.2 Smoothed Objective with Barrier Function

To efficiently and accurately solve the convex constrained optimization problem (3.1), we adopt the *Interior-Point Method* (IPM) (Wright et al., 1999) that solves a sequence of relaxed problems with decreasing $\mu > 0$ to reliably converge to a solution of the exact LCS $f_{\mu=0}$.

We show that the softened LCS is the optimality condition of a barrier-smoothed objective with the following lemma. We defer all the proofs in this paper to Appendix A.

Lemma 3.3 (Primal Problem with Log-Barrier Function)**.** The softened LCS (3.1) with $\mu \geq 0$ is the first-order optimality condition of the following program:

$$\begin{aligned} \min_{\lambda_t \geq \vec{0}, \epsilon_t \geq \vec{0}} \quad & \lambda_t^\top \epsilon_t - \mu \sum_{i=1}^{d_\lambda} \left(\log \lambda_t^{(i)} + \log \epsilon_t^{(i)} \right) \\ \text{s.t.} \quad & Dx_t + Eu_t + F\lambda_t + d = \epsilon_t, \\ & Ax_t + Bu_t + C\lambda_t + c = x_{t+1}, \end{aligned} \tag{3.2}$$

where $\lambda_t^{(i)}, \epsilon_t^{(i)}$ are the i-th elements of vector $\lambda_t, \epsilon_t \in \mathbb{R}^{d_\lambda}$.

Lemma 3.3 indicates that the softened LCS is in fact the perturbed Karush–Kuhn–Tucker (KKT) conditions, where the perturbation corresponds to smoothing the objective with barrier functions. By replacing the hard contact constraints in the LCS $f_{\mu=0}$, the logarithmic barrier functions in (3.2) discourages the solution to reach the boundary of the polytope constructed by the hard constraints. Therefore, μ restrains the solution within the analytic center of the constraint polytope and is a central-path parameter.

The barrier terms can be thought of as the potential of a force field whose strength is inversely proportional to the distance to the constraint boundary (Boyd et al., 2004). When applying IPM with a sequence of central-path parameters, the intermediate problems with $\mu > 0$ achieve a smoothing effect similar to the "force-at-a-distance" relaxation (Pang et al., 2022) of the complementarity constraints. In other words, μ controls both the *stiffness* and the *accuracy* of the

softened LCS model f_μ. In what follows, we will show that both properties are determining factors for the quality of first-order gradient estimation and the convergence of the resulting policy gradient algorithm.

4 Model-Based First-Order Policy Gradient

In this section, we first provide a general framework of model-based First-Order Policy Gradient (FOPG). Then we establish the convergence of model-based FOPG and study the relationship between its convergence rate and the gradient bias, variance. Then we analyze the relationship between the gradient variance and the model stiffness, as well as the stiffness of complementarity-based models. Based on our analysis, we find that non-smooth behaviors of contact events can lead to optimization difficulties, which motivates us to analytically smooth the system.

4.1 Framework

In Algorithm 1, we provide the pseudocode of model-based FOPG, where two update procedures are performed iteratively. Namely, the model and the policy are updated in every iteration $n \in [N]$, which gives us sequences of $\{f_{\psi_n}\}_{n\in[N]}$ and $\{\pi_{\theta_t}\}_{t\in[T+1]}$, respectively.

Algorithm 1 Model-Based First-Order Policy Gradient

Input: Number of iterations N, transition data set $\mathcal{D} = \varnothing$
1: **for** iteration $n \in [N]$ **do**
2: Update the model parameter ψ_n by minimizing (4.1)
3: Update the policy parameter θ_n by (4.3)
4: Execute $\pi_{\theta_{n+1}}$ and update $\mathcal{D}$
5: **end for**
6: **Output:** $\{\pi_{\theta_n}\}_{n\in[N]}$

Model Update. A forward state-predictive model is learned from data $\mathcal{D} = \{(x_t^*, u_t^*, x_{t+1}^*)\}_{t=1}^T$. For rigid-body systems that experience hard contact, we learn a physically grounded model $x_{t+1} = f(x_t, u_t; \psi)$ where the state $x_t \in \mathbb{R}^{d_x}$ is the system's configuration (including velocity v_t, coordinate q_t, etc.), and f returns the solution of (2.3) constrained by (2.4), (2.5). Instead of parameterized by a black-box neural network, ψ contains all *estimated* physics data such as friction coefficient and parameters of each body. The model training loss is as follows, minimized by random search:

$$L(\psi; \mathcal{D}) = \sum_{t=1}^{T} \frac{1}{2} \left\| f(x_t^*, u_t^*; \psi) - x_{t+1}^* \right\|_2^2. \tag{4.1}$$

Policy Update. Consider optimizing a stochastic policy $u \sim \pi_\theta(\cdot|x)$ in continuous action spaces, or equivalently $u = \pi_\theta(x, \varsigma)$ with noise $\varsigma \sim p(\varsigma)$. The first-order policy gradient at iteration n is given by linking together the reward, model, policy, and differentiating through the model-generated trajectories:

$$\widehat{\nabla}_\theta \mathcal{J}(\pi_{\theta_n}) = \frac{1}{M} \sum_{m=1}^{M} \nabla_\theta \left(\sum_{t=0}^{H-1} \gamma^t \cdot r(x_{t,m}, u_{t,m}) \right), \tag{4.2}$$

where M is the batch size, $x_{0,m} \sim \zeta$, $u_{t,m} = \pi(x_{t,m}, \varsigma_m)$, $\varsigma_m \sim p(\varsigma)$, and $x_{t+1,m} = f(x_{t,m}, u_{t,m})$.

The update rule for the policy parameter θ with learning rate η is as follows:

$$\theta_{n+1} \leftarrow \theta_n + \eta \cdot \widehat{\nabla}_\theta \mathcal{J}(\pi_{\theta_n}). \tag{4.3}$$

4.2 Convergence of Model-Based FOPG

To begin our analysis, we impose a common regularity condition on the policy functions following previous works (Xu et al., 2019; Pirotta et al., 2015; Zhang et al., 2020; Agarwal et al., 2021). The assumption below essentially ensures the smoothness of the objective $\mathcal{J}(\pi_\theta)$, which is required by most existing studies on the policy gradient methods (Wang et al., 2019; Bastani, 2020; Agarwal et al., 2020).

Assumption 4.1 (Lipschitz Continuous Policy Gradient)**.** Assume that $\nabla_\theta \mathcal{J}(\pi_\theta)$ is L-Lipschitz continuous in θ, such that $\|\nabla_\theta \mathcal{J}(\pi_{\theta_1}) - \nabla_\theta \mathcal{J}(\pi_{\theta_2})\|_2 \le L\|\theta_1 - \theta_2\|_2$.

We characterize the convergence of model-based FOPG by first providing the following proposition.

Theorem 4.2 (Convergence to Stationary Points)**.** Define the gradient bias b_n and variance v_n at iteration n as

$$b_n := \left\| \nabla_\theta \mathcal{J}(\pi_{\theta_n}) - \mathbb{E}\left[\widehat{\nabla}_\theta \mathcal{J}(\pi_{\theta_n})\right] \right\|_2,$$
$$v_n := \mathbb{E}\left[\left\| \widehat{\nabla}_\theta \mathcal{J}(\pi_{\theta_n}) - \mathbb{E}\left[\widehat{\nabla}_\theta \mathcal{J}(\pi_{\theta_n})\right] \right\|_2^2 \right].$$

Denote $\delta := \sup \|\theta\|_2$ and $c := (\eta - L\eta^2)^{-1}$. It then holds for $N \ge 4L^2$ that

$$\min_{n\in[N]} \mathbb{E}\left[\left\| \nabla_\theta \mathcal{J}(\pi_{\theta_n}) \right\|_2^2 \right] \le \frac{4c}{N} \cdot \mathbb{E}\left[\mathcal{J}(\pi_{\theta_N}) - \mathcal{J}(\pi_{\theta_1}) \right] + \frac{4}{N} \left(\sum_{n=0}^{N-1} c(2\delta \cdot b_n + \frac{\eta}{2} \cdot v_n) + b_n^2 + v_n \right).$$

Theorem 4.2 shows the reliance between the convergence error and the variance, bias of the gradient estimators. In general, to guarantee the convergence of model-based FOPG, we have to control both the variance and the bias to the sublinear growth rate. Before studying the upper bound of b_n and v_n, we make the following Lipschitz assumption, which is adopted in various previous works (Pirotta et al., 2015; Clavera et al., 2020; Li et al., 2021).

Assumption 4.3 (Lipschitz Continuity)**.** Assume the policy, model, and reward are L_π, L_f, L_r Lipschitz continuous.

4.3 Gradient Variance and LCS Stiffness

Denote $\widetilde{L}_g := \max\{L_g, 1\}$ for any function g. We have the following result for the variance of FOPG.

Theorem 4.4 (Gradient Variance)**.** Under Assumption 4.3, at iteration $n \in [N]$, the gradient variance of FOPG satisfies

$$v_n \leq O\Big(H^4 \widetilde{L}_f^{4H} \widetilde{L}_\pi^{4H} / M\Big). \tag{4.4}$$

We observe that the variance upper bound has polynomial dependence on the Lipschitz of the model and policy, where the degrees are linear in the effective horizon. This makes intuitive sense: When the system is chaotic (Bollt, 2000), as measure by the Jacobian of the dynamical system, the stochasticity during training can lead to diverging trajectories and gradient directions, causing large gradient variance. The optimization difficulties imposed by non-smooth models, e.g. the hard contact models, result in slow convergence or training failure even in simple toy tasks (Parmas et al., 2018; Suh et al., 2022a).

The above analysis holds for general model-based FOPG. When adopting the complementarity-based contact model f_μ, studying its stiffness, i.e. the Lipschitz L_{f_μ}, is especially important since they are inherently non-smooth or discontinuous at local mode-switching points. We characterize the stiffness of the softened LCS with the following theorem.

Theorem 4.5 (Stiffness of the Softened LCS)**.** Let $\|\cdot\|_F$ denote the matrix Frobenius norm and define $\varepsilon := \sup \|Dx_t + Eu_t + d\|_2^2/(2\|F\|_F^2)$. Under Assumption 3.2, the Lipschitz L_{f_μ} of the model f_μ defined in (3.1) satisfies

$$L_{f_\mu} \leq (\|A\|_F + \|B\|_F) + d_\lambda^2 \|C\|_F (\|D\|_F + \|E\|_F) \cdot l(\mu),$$

where $l(\mu)$ is determined by μ and is lower bounded by

$$l(\mu) \geq \frac{\varepsilon}{\mu} + \frac{1}{\|F\|_F} + \varepsilon \sqrt{\frac{1}{\mu^2} + \frac{2}{\varepsilon \mu \|F\|_F}}.$$

Theorem 4.5 indicates that the model stiffness is largely determined by the central-path parameter μ: The upper bound of L_{f_μ} (and thus of the variance (4.4)) is at least inversely proportional to μ. This is problematic when performing first-order policy gradient based on the softened LCS model f_μ: The accurate dynamics are obtained when solving the exact LCP ($\mu \to 0$), which, however, causes the gradient variance to explode since $l(\mu) \to \infty$. The optimization challenges, e.g. chaotic and non-smooth landscapes, are posed even when contact occurs occasionally in a full model unroll.

5 Contact-Aware Analytic Barrier Smoothing

5.1 Method

A natural idea to alleviate the exploding FOPG variance issue is to differentiate through the intermediate solution of IPM when calculating the gradient in (4.2). In other words, we can set a positive stopping criteria μ_{sc} such that the IPM iterations are terminated once $\mu \approx \mu_{\text{sc}}$. Details including the pseudocode are deferred to Appendix B. According to Lemma 3.3, μ-softened systems correspond to the smoothed objectives with log-barrier functions. For this reason, we call this vanilla method *Analytic Barrier Smoothing*.

Unfortunately, vanilla analytic smoothing with a constantly large μ_{sc} can lead to a huge gradient bias since the generated trajectories will *not* obey the physics laws. Therefore, to achieve a good convergence in Thm. 4.2, additional care must be taken to trade-off between the variance and bias.

In this work, we propose to control the FOPG gradient bias using *contact-aware* analytic barrier smoothing: Instead of a constant μ_{sc}, we set it to be *adaptive* $\mu_{\text{sc}} = \mu(x_t, u_t) > 0$, whose value scales *inversely* with the minimum distance-to-obstacle $|\phi(x_t, u_t)|$ of the *inactive impact contacts*.

This contact-aware design is based on the observation that the stiffness of complementarity-based models mainly comes from the sudden change of the impact force when the penetration first arises. For example, in systems of Fig. 1(a) and 1(b), the velocity is continuous everywhere except at the hard contact point $z = 0$. For system states that contain the velocity information, the dynamics are stiff around $z = 0$ (see Sec. 7.1 for illustrations). Therefore, when performing FOPG, we only need *local* smoothing near the inactive impact contact to avoid large variance, while maintaining *globally* accurate gradients for a small overall bias.

The choice of $\mu(x_t, u_t)$ can be problem-dependent, as long as it decreases with $|\phi(x_t, u_t)|$ (e.g., we use (7.1) in our experiments). In the following section, we show that analytic barrier smoothing has a close relationship with randomized smoothing and, when the contact-aware $\mu(x_t, u_t)$ takes certain forms, enjoys small gradient bias.

5.2 Analysis

Since we are interested in controlling the system stiffness and reducing the gradient variance brought by the impact contact, we study frictionless systems with a single contact point in this section. This simplifies our analysis by reducing d_λ to 1. Although the results might generalize to broader settings, their forms are beyond the scope of this paper.

As a first step, we build the connection between the proposed *contact-aware analytic barrier smoothing* and *randomized smoothing* (Suh et al., 2022a;b; Pang et al., 2022), which samples and averages the stochastic gradient. We show that these two smoothing techniques are identical in principle.

Proposition 5.1 (Equivalence with Randomized Smoothing)**.** Denote $z_t := Dx_t + Eu_t + d \in \mathbb{R}$. Recall that the solution of the exact LCP is $S_{\mu=0}(z_t)$ and the analytically smoothed LCP solution is $S_{\mu(z_t)}(z_t)$ (see Defn. 3.1). For any centering function $\mu(z_t)$, analytic smoothing is equivalent to randomized smoothing: $S_{\mu(z_t)}(z_t) =$

$\mathbb{E}_{w\sim\rho(w)}[S_{\mu=0}(z_t+w)]$, where $\rho(w)=\nabla_w^2 S_{\mu(z_t)}(w)$.

The above proposition shows that analytic barrier smoothing is inherently smoothing the contact force λ_t (with respect to z_t), and thus smoothing the dynamics $x_{t+1}=f_\mu(x_t,u_t)$ as x_t,u_t are prefixed. More importantly, by choosing a proper adaptive central-path parameter $\mu(z_t)$, the proposed method can cover any randomized smoothing method, while avoiding its drawbacks when calculating first-order gradients, which we will discuss in more detail.

As a consequence of Proposition 5.1, we can work directly on the randomization-smoothed model when studying the bias of analytic smoothing. This gives us the following results adapted from the analysis on randomized smoothing (Pang et al., 2022).

Proposition 5.2 (Smoothing as Linearization Minimizer)**.** Define the error function as the σ-Gaussian tail integral $\mathrm{erf}(y;\sigma^2) := \int_y^\infty 1/(\sqrt{2\pi}\sigma)e^{-y^2/\sigma^2}$. Set the z_t-adaptive central-path parameter as $\mu(z_t)=\kappa\cdot(z_t+F\kappa)$, where

$$\kappa := z_t\cdot\mathrm{erf}(z_t,\sigma)+e^{-z_t^2/(2\sigma)}/\sqrt{\pi}+c_1 z_t+c_2, \quad (5.1)$$

and $c_1,c_2\in\mathbb{R}$ are tunable constants. Consider the problem of regressing the exact LCP solution $S_{\mu=0}$ with parameters (K,W) such that the residual around z_t distributed according to Gaussian is minimized, formally:

$$\delta=\min_{K,W}\mathbb{E}_{w\sim\mathcal{N}(0,\sigma)}\Big[\big|S_{\mu=0}(z_t+w)-Ww-K\big|\Big].$$

The K^*,W^* that achieve the minimum are the analytically smoothed solution and its gradient, respectively:

$$K^*=S_{\mu(z_t)}(z_t),\quad W^*=\nabla_z S_{\mu(z_t)}(z_t).$$

The above proposition shows that analytic smoothing is the best linear approximation of the LCP solution around z_t. Therefore, with a small approximation error, we can conclude the model gradient bias of analytic barrier smoothing.

In Figure 1(c), we observe that $\mu(z_t)$ defined in (5.1) is contact-aware as it is positive only when around the contact point $z_t=0$. This design supports our intuition: When the body is away from contact, we can safely solve the LCP and get accurate simulations; When experiencing contact, the proposed method smooths the LCP to obtain non-stiff local dynamics. This is also obvious from Figure 1(d): λ_t is more accurate at contact-free regions, while achieving the "force-at-a-distance" relaxation around $z_t=0$.

Theorem 5.3 (Bias of Analytic Smoothing)**.** With the same definition of $\mu(z_t)$ in Proposition 5.2, the gradient of the softened LCS model $f_{\mu(z_t)}$ approximately matches the gradient of LCS $f_{\mu=0}$, with the bias upper bounded by

$$\big\|\nabla f_{\mu=0}-\nabla f_{\mu(z_t)}\big\|_2 \le \|C\|_F(\|D\|_F+\|E\|_F)\cdot\Big(\frac{\sigma F^2\mathcal{Q}(3/4)}{2}+\frac{12\delta+\varsigma}{\sigma\mathcal{Q}(2/3)}\Big),$$

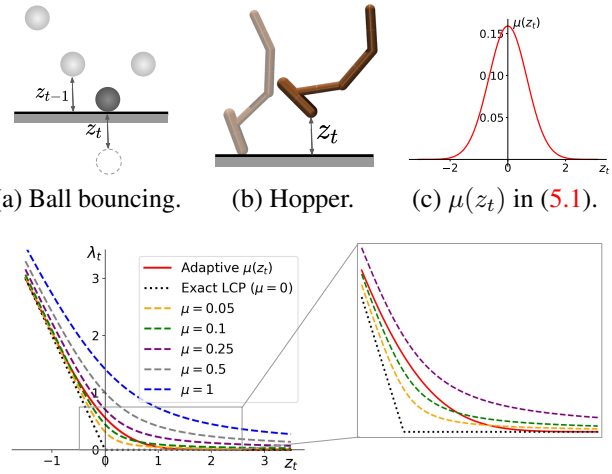

(a) Ball bouncing. (b) Hopper. (c) $\mu(z_t)$ in (5.1).

(d) Contact impulses λ_t of the exact and the softened LCP, including constant μ and the contact-aware adaptive $\mu(z_t)$.

Figure 1. 1(a), 1(b): Example systems. The dashed circle in 1(a) arises penetration $z_t<0$, where the contact force $\lambda_t>0$ pushes the ball to be above the ground. 1(c): Plot of the proposed adaptive $\mu(z_t)$. 1(d): Contact force comparison. The proposed $\mu(z_t)$ is contact-aware and has a better balance of stiffness smoothing and bias reduction: Around the contact point $z=0$, adaptive $\mu(z_t)$ gives smoother dynamics (compared to $\mu\le 0.1$) and meanwhile best approximates the exact LCP at contact-free regions $z>0$.

where we define $\varsigma := 1/\sqrt{\pi}+c_2$ and $\mathcal{Q}:[0,1]\to\mathbb{R}$ is the inverse of the cumulative distribution function (or quantile function) of the standard normal distribution, $\mathcal{Q}(3/4)\approx 0.67$, $\mathcal{Q}(2/3)\approx 0.43$.

In Thm. 5.3, we bound the gradient bias of analytic barrier smoothing when the contact-aware $\mu(z_t)$ takes specific forms. If the model parameters ψ are accurately fitted with supervised learning, i.e. $f_{\mu=0}\approx f^*$, the softened LCS $f_{\mu(z_t)}$ and its gradient achieves the best linearization error and has small gradient bias b_n.

Discussion on Randomized Smoothing. Although equivalence can be established between analytic smoothing $f_{\mu>0}(x)$ and randomized smoothing $\mathbb{E}_{w\sim\rho}[f_{\mu=0}(x+w)]$, the latter suffers from the empirical bias (Suh et al., 2022b;a) and the noisy gradients (Howell et al., 2022).

The empirical bias phenomenon happens under discontinuities or stiffness (see Fig. 7(a)). Even if the system is non-stiff, sampling and averaging the noise-induced gradients is noisy and computationally expensive. In contrast, analytic smoothing by directly differentiating through the softened system $f_{\mu>0}$ prevents the above issues.

6 Related Work

Differentiable Simulation. The physics-guided (Jiang et al., 2018; Pizzuto & Mistry, 2021) complementarity-based

model that is used in this work is adopted in various differentiable hard-contact engines, such as Dojo (Howell et al., 2022), DART (Werling et al., 2021), and Bullet (Heiden et al., 2021). The (sub-)gradients of simulation outcomes w.r.t. control actions are readily available in these differentiable simulators. However, the extreme curvatures of contact events prevent the (sub-)gradients to be effective when performing FOPG, and our method serves as a potential solution. On the other hand, simulators such as MuJoCo (Todorov et al., 2012) and PhysX, implement soft contacts and can generate physics-violated behaviors (Howell et al., 2022). Besides, their non-differentiable nature requires expensive finite-difference to obtain the first-order gradients.

Policy Gradient Methods. The zeroth-order policy gradient methods include REINFORCE (Williams, 1992) and actor-critic (Sutton et al., 1999; Kakade, 2001; Kakade & Langford, 2002; Degris et al., 2012), where the convergence results are established in recent works (Agarwal et al., 2021; Wang et al., 2019; Bhandari & Russo, 2019; Liu et al., 2019). However, less attention has been focused on first-order policy gradient. The optimization difficulties, such as discontinuous contact behaviors and the curse of chaos (Parmas et al., 2018; Metz et al., 2021; Xu et al., 2022), prevent the widespread of FOPG even in differentiable simulation. To alleviate this issue, (Suh et al., 2022b;a; Pang et al., 2022) proposed randomized smoothing, and (Xu et al., 2022) proposed to shorten the optimization horizon. In this work, we focus on the naive implementation of FOPG. Modifications from previous works can be naturally integrated, e.g. using an additional critic as the tail estimation (Clavera et al., 2020), minimizing the model gradient error (Li et al., 2021), or adding actor entropy loss (Amos et al., 2021).

7 Experiments

7.1 Contact Behaviors and System Stiffness

We first provide the insight behind analytic smoothing. In Figure 2, we plot the dynamics and derivatives of the velocity w.r.t. coordinate in the ball bouncing example, where the ball is thrown with an initial velocity, subjected to the gravity and impact force (when hitting the ground).

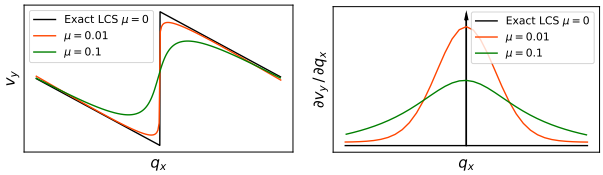

(a) Dynamics. (b) Derivative.

Figure 2. Contact behaviors in the Fig. 1(a) ball bouncing example. 2(a): The vertical velocity v_y w.r.t. the x-coordinate q_x in the exact LCS and in the μ-smoothed system. 2(b): Derivative of v_y w.r.t. q_x. The black arrow represents the impulse function, i.e. $\partial v_y / \partial q_x = \infty$ at the contact point and $= -g$ (gravity) elsewhere.

In Fig. 2(a), the velocity is discontinuous at the contact point due to the sudden change of the impact force γ from 0 to a positive value. This results in the stiffness of the system $f_{\mu=0}(x)$ where the state $x = (q_x, v_y)$. As the basis of more complex behaviors, similar contact events happen in almost all robotic tasks. With analytic smoothing, the dynamics become less stiff with larger relaxation μ.

7.2 First-Order Gradient Variance

Consider the ball bouncing dynamics with additional Gaussian noise that resembles the stochasticity during training, such as action and transition noise. In the right figure, we plot the maximum variance of first-order reparameterization gradients and zeroth-order likelihood ratio (LR) gradients. We observe that stiff systems with small μ lead to large first-order gradient variance. This is due to the curse of chaos that for non-smooth dynamics, the stochasticity can lead to diverging trajectories and gradients. Here, LR gradients are parameterized with Gaussian, following evolutionary strategies (Salimans et al., 2017; Mania et al., 2018). Although the LR gradient is better behaved under stiffness as it is solely based on function evaluations, it is known to scale poorly when the dimensionality increases in more complex tasks (see Section 7.3).

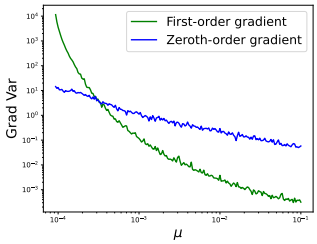

Figure 3. Max gradient variance of the noisy contact dynamics.

We then conduct experiments in the Dojo (Howell et al., 2022) physics engine, which enables differentiable simulation with hard contact. For now, we use the ground-truth physics parameters. We plot the mean gradient variance during the FOPG training in locomotion tasks in Figure 4.

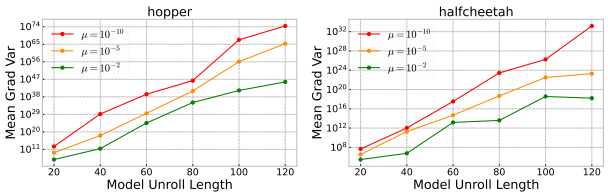

Figure 4. The mean gradient variance with different model unroll lengths when changing the μ value.

We observe that the gradient variance of FOPG can explode in exponential order with respect to the model unroll lengths. When μ increases, which indicates a larger Lipschitz constant of the complementarity-based model, the variance decreases. This supports our result in Theorem 4.4.

In the following sections, we conduct the Dojo experiments by learning the physical parameters ψ, including the friction

coefficient, the spring coefficient of the joints, and the motor gear coefficients.

7.3 Contact-Aware Analytic Smoothing

Results in the last section indicate that analytically smoothed dynamics are preferred if we would like the gradient variance to be small and the optimization to be non-chaotic. However, the gradient of smoothed models will be biased, where the trade-off between variance and bias must be taken. Here, we evaluate analytic smoothing equipped with the contact-aware $\mu(x_t, u_t)$ that takes the following form:

$$\mu = 10^{-2}\big(10\big(\min_{i\in\mathcal{I}}\{|\phi(x_t,u_t)^{(i)}|, 1\}\big)^2 + 1\big)^{-4}, \quad (7.1)$$

where $\mathcal{I} := \{1 \le i \le c \,|\, \gamma_{t-1}^{(i)} \le 1\}$ represents the set of inactive impact contact points. The above design ensures that $\mu \approx 10^{-10}$ when all impact contacts are active or the distance between contact and obstacles is large; and $\mu \approx 10^{-2}$ when this distance is small.

In Figure. 5, we report the performance of the proposed method in two locomotion tasks. Compared with constant μ (or μ_{sc}), contact-aware analytic barrier smoothing has faster convergence and higher return. We also evaluate *Augmented Random Search* (ARS) (Mania et al., 2018), which is equivalent to parameterizing the zeroth-order gradient with Gaussian. The results reveal the potential of model-based FOPG.

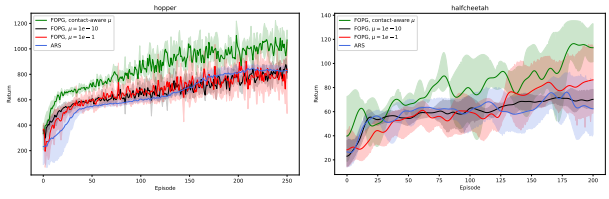

Figure 5. Performance in the Dojo locomotion tasks.

7.4 Ablation Studies

Gradient Bias. We have shown that a small μ corresponding to stiff systems leads to a large gradient variance. In this part, we verify that the increasing gradient bias is to be blamed that the performance obtained by setting a large μ lags behind contact-aware analytic smoothing.

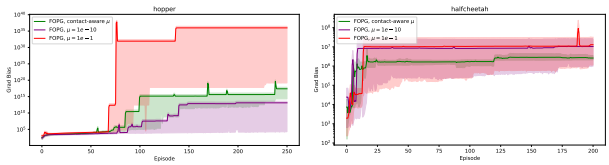

Figure 6. Ablation on the gradient bias.

Different Smoothing Mechanisms. Figure 7(a) illustrates the derivatives of the *impact* contact dynamics in the above ball-bouncing example, from which we observe the empirical bias phenomenon of randomized smoothing. Specifically, the dynamics in Fig. 2(a) have a constant gradient $(-g)$ everywhere except at the contact point. The AS gradient successfully approximates the unit impulse at contact, while the RS gradient is $-g$ and has a large bias. For frictional contact 7(b), the RS gradient is both noisy and expensive to compute due to its sampling and averaging process. Similar observations are also documented in (Howell et al., 2022; Suh et al., 2022a).

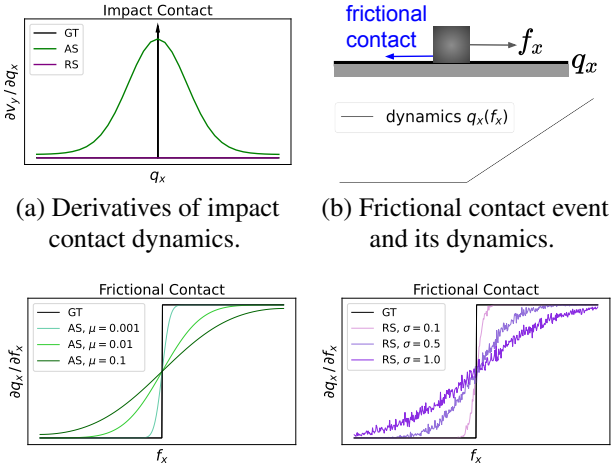

(a) Derivatives of impact contact dynamics.

(b) Frictional contact event and its dynamics.

(c) Derivatives of frictional contact dynamics.

Figure 7. Comparison between the proposed Analytic Smoothing (AS) and Randomized Smoothing (RS) in the two types of contact dynamics (impact and friction). RS gradient is biased and noisy.

8 Conclusion

In this work, we study the model-based First-Order Policy Gradient (FOPG) methods in robotic contact dynamics. We focus on complementarity-based physical models that can efficiently fit the contact behaviors, whose dynamics are with extreme curvatures. We show that the convergence of FOPG methods relies on the gradient variance and bias, and the stiff complementarity models can cause optimization difficulties due to the exploding variance. Therefore, we propose *Analytic Barrier Smoothing* to reduce the model stiffness and variance, and the bias is controlled by adopting the contact-aware central-path parameter. We provide the upper bound of the gradient variance and bias of the proposed method. Our result also established the reliance on the stiffness of the softened linear complementarity systems, as well as the equivalence between analytic smoothing and randomized smoothing. Our work also opens some new problems. It would be interesting to investigate how the soft contact dynamics in systems like MuJoCo affect the model learning and policy gradients. Besides, we analyze the bias of our method in simplified settings. We leave the extension to general contact systems for future work.

References

Agarwal, A., Kakade, S. M., Lee, J. D., and Mahajan, G. Optimality and approximation with policy gradient methods in markov decision processes. In *Conference on Learning Theory*, pp. 64–66. PMLR, 2020.

Agarwal, A., Kakade, S. M., Lee, J. D., and Mahajan, G. On the theory of policy gradient methods: Optimality, approximation, and distribution shift. *Journal of Machine Learning Research*, 22(98):1–76, 2021.

Amos, B., Stanton, S., Yarats, D., and Wilson, A. G. On the model-based stochastic value gradient for continuous reinforcement learning. In *Learning for Dynamics and Control*, pp. 6–20. PMLR, 2021.

Anitescu, M. and Potra, F. A. A time-stepping method for stiff multibody dynamics with contact and friction. *International journal for numerical methods in engineering*, 55(7):753–784, 2002.

Aydinoglu, A., Preciado, V. M., and Posa, M. Contact-aware controller design for complementarity systems. In *2020 IEEE International Conference on Robotics and Automation (ICRA)*, pp. 1525–1531. IEEE, 2020.

Aydinoglu, A., Sieg, P., Preciado, V. M., and Posa, M. Stabilization of complementarity systems via contact-aware controllers. *IEEE Transactions on Robotics*, 2021.

Bastani, O. Sample complexity of estimating the policy gradient for nearly deterministic dynamical systems. In *International Conference on Artificial Intelligence and Statistics*, pp. 3858–3869. PMLR, 2020.

Belkin, M., Hsu, D., Ma, S., and Mandal, S. Reconciling modern machine-learning practice and the classical bias–variance trade-off. *Proceedings of the National Academy of Sciences*, 116(32):15849–15854, 2019.

Bhandari, J. and Russo, D. Global optimality guarantees for policy gradient methods. *arXiv preprint arXiv:1906.01786*, 2019.

Bollt, E. M. Controlling chaos and the inverse frobenius–perron problem: global stabilization of arbitrary invariant measures. *International Journal of Bifurcation and Chaos*, 10(05):1033–1050, 2000.

Boyd, S., Boyd, S. P., and Vandenberghe, L. *Convex optimization*. Cambridge university press, 2004.

Chua, K., Calandra, R., McAllister, R., and Levine, S. Deep reinforcement learning in a handful of trials using probabilistic dynamics models. *Advances in neural information processing systems*, 31, 2018.

Clavera, I., Fu, V., and Abbeel, P. Model-augmented actor-critic: Backpropagating through paths. *arXiv preprint arXiv:2005.08068*, 2020.

Degris, T., White, M., and Sutton, R. S. Off-policy actor-critic. *arXiv preprint arXiv:1205.4839*, 2012.

Drumwright, E. and Shell, D. A. Extensive analysis of linear complementarity problem (lcp) solver performance on randomly generated rigid body contact problems. In *2012 IEEE/RSJ International Conference on Intelligent Robots and Systems*, pp. 5034–5039. IEEE, 2012.

Freeman, C. D., Frey, E., Raichuk, A., Girgin, S., Mordatch, I., and Bachem, O. Brax–a differentiable physics engine for large scale rigid body simulation. *arXiv preprint arXiv:2106.13281*, 2021.

Geilinger, M., Hahn, D., Zehnder, J., Bächer, M., Thomaszewski, B., and Coros, S. Add: Analytically differentiable dynamics for multi-body systems with frictional contact. *ACM Transactions on Graphics (TOG)*, 39(6):1–15, 2020.

Grimmett, G. and Stirzaker, D. *Probability and random processes*. Oxford university press, 2020.

Heiden, E., Millard, D., Coumans, E., Sheng, Y., and Sukhatme, G. S. Neuralsim: Augmenting differentiable simulators with neural networks. In *2021 IEEE International Conference on Robotics and Automation (ICRA)*, pp. 9474–9481. IEEE, 2021.

Hochlehnert, A., Terenin, A., Sæmundsson, S., and Deisenroth, M. Learning contact dynamics using physically structured neural networks. In *International Conference on Artificial Intelligence and Statistics*, pp. 2152–2160. PMLR, 2021.

Howell, T. A., Cleac'h, S. L., Kolter, J. Z., Schwager, M., and Manchester, Z. Dojo: A differentiable simulator for robotics. *arXiv preprint arXiv:2203.00806*, 2022.

Jiang, Y., Sun, J., and Liu, C. K. Data-augmented contact model for rigid body simulation. *arXiv preprint arXiv:1803.04019*, 2018.

Jin, W., Aydinoglu, A., Halm, M., and Posa, M. Learning linear complementarity systems. In *Learning for Dynamics and Control Conference*, pp. 1137–1149. PMLR, 2022.

Kaiser, L., Babaeizadeh, M., Milos, P., Osinski, B., Campbell, R. H., Czechowski, K., Erhan, D., Finn, C., Kozakowski, P., Levine, S., et al. Model-based reinforcement learning for atari. *arXiv preprint arXiv:1903.00374*, 2019.

Kakade, S. and Langford, J. Approximately optimal approximate reinforcement learning. In *In Proc. 19th International Conference on Machine Learning*. Citeseer, 2002.

Kakade, S. M. A natural policy gradient. *Advances in neural information processing systems*, 14, 2001.

Li, C., Wang, Y., Chen, W., Liu, Y., Ma, Z.-M., and Liu, T.-Y. Gradient information matters in policy optimization by back-propagating through model. In *International Conference on Learning Representations*, 2021.

Liu, B., Cai, Q., Yang, Z., and Wang, Z. Neural trust region/proximal policy optimization attains globally optimal policy. *Advances in neural information processing systems*, 32, 2019.

Mania, H., Guy, A., and Recht, B. Simple random search provides a competitive approach to reinforcement learning. *arXiv preprint arXiv:1803.07055*, 2018.

Mehrotra, S. On the implementation of a primal-dual interior point method. *SIAM Journal on optimization*, 2(4):575–601, 1992.

Metz, L., Freeman, C. D., Schoenholz, S. S., and Kachman, T. Gradients are not all you need. *arXiv preprint arXiv:2111.05803*, 2021.

Mohamed, S., Rosca, M., Figurnov, M., and Mnih, A. Monte carlo gradient estimation in machine learning. *J. Mach. Learn. Res.*, 21(132):1–62, 2020.

Nagabandi, A., Kahn, G., Fearing, R. S., and Levine, S. Neural network dynamics for model-based deep reinforcement learning with model-free fine-tuning. In *2018 IEEE International Conference on Robotics and Automation (ICRA)*, pp. 7559–7566. IEEE, 2018.

Pang, T., Suh, H., Yang, L., and Tedrake, R. Global planning for contact-rich manipulation via local smoothing of quasi-dynamic contact models. *arXiv preprint arXiv:2206.10787*, 2022.

Parmar, M., Halm, M., and Posa, M. Fundamental challenges in deep learning for stiff contact dynamics. In *2021 IEEE/RSJ International Conference on Intelligent Robots and Systems (IROS)*, pp. 5181–5188. IEEE, 2021.

Parmas, P., Rasmussen, C. E., Peters, J., and Doya, K. Pipps: Flexible model-based policy search robust to the curse of chaos. In *International Conference on Machine Learning*, pp. 4065–4074. PMLR, 2018.

Pfrommer, S., Halm, M., and Posa, M. Contactnets: Learning discontinuous contact dynamics with smooth, implicit representations. In *Conference on Robot Learning*, pp. 2279–2291. PMLR, 2021.

Pirotta, M., Restelli, M., and Bascetta, L. Policy gradient in lipschitz markov decision processes. *Machine Learning*, 100(2):255–283, 2015.

Pizzuto, G. and Mistry, M. Physics-penalised regularisation for learning dynamics models with contact. In *Learning for Dynamics and Control*, pp. 611–622. PMLR, 2021.

Salimans, T., Ho, J., Chen, X., Sidor, S., and Sutskever, I. Evolution strategies as a scalable alternative to reinforcement learning. *arXiv preprint arXiv:1703.03864*, 2017.

Schrittwieser, J., Antonoglou, I., Hubert, T., Simonyan, K., Sifre, L., Schmitt, S., Guez, A., Lockhart, E., Hassabis, D., Graepel, T., et al. Mastering atari, go, chess and shogi by planning with a learned model. *Nature*, 588(7839): 604–609, 2020.

Suh, H., Simchowitz, M., Zhang, K., and Tedrake, R. Do differentiable simulators give better policy gradients? *arXiv preprint arXiv:2202.00817*, 2022a.

Suh, H. J. T., Pang, T., and Tedrake, R. Bundled gradients through contact via randomized smoothing. *IEEE Robotics and Automation Letters*, 7(2):4000–4007, 2022b.

Sutton, R. S., McAllester, D., Singh, S., and Mansour, Y. Policy gradient methods for reinforcement learning with function approximation. *Advances in neural information processing systems*, 12, 1999.

Tassa, Y. and Todorov, E. Stochastic complementarity for local control of discontinuous dynamics. 2010.

Todorov, E., Erez, T., and Tassa, Y. MuJoCo: A physics engine for model-based control. In *2012 IEEE/RSJ international conference on intelligent robots and systems*, pp. 5026–5033. IEEE, 2012.

Wang, L., Cai, Q., Yang, Z., and Wang, Z. Neural policy gradient methods: Global optimality and rates of convergence. *arXiv preprint arXiv:1909.01150*, 2019.

Werling, K., Omens, D., Lee, J., Exarchos, I., and Liu, C. K. Fast and feature-complete differentiable physics engine for articulated rigid bodies with contact constraints. In *Robotics: Science and Systems*, 2021.

Williams, R. J. Simple statistical gradient-following algorithms for connectionist reinforcement learning. *Machine learning*, 8(3):229–256, 1992.

Wright, S., Nocedal, J., et al. Numerical optimization. *Springer Science*, 35(67-68):7, 1999.

Xu, J., Makoviychuk, V., Narang, Y., Ramos, F., Matusik, W., Garg, A., and Macklin, M. Accelerated policy learning with parallel differentiable simulation. *arXiv preprint arXiv:2204.07137*, 2022.

Xu, P., Gao, F., and Gu, Q. Sample efficient policy gradient methods with recursive variance reduction. *arXiv preprint arXiv:1909.08610*, 2019.

Zhang, K., Koppel, A., Zhu, H., and Basar, T. Global convergence of policy gradient methods to (almost) locally optimal policies. *SIAM Journal on Control and Optimization*, 58(6):3586–3612, 2020.

A Proofs

A.1 Proof of Lemma 3.3

Proof. Corresponding to the constrained optimization problem (3.2) we can introduce the multipliers ι and form the Lagrangian function by

$$L(\lambda_t, \epsilon_t, \iota) = \lambda_t^\top \epsilon_t - \mu \sum_{i=1}^{n_\lambda} \big(\log \lambda_t^{(i)} + \log \epsilon_t^{(i)}\big) + \iota^\top (Dx_t + Eu_t + F\lambda_t + d - \epsilon_t).$$

Here, we omit the last equality constraint in (3.2) since x_{t+1} can be directly calculated when λ_t is obtained.

We have from the Karush–Kuhn–Tucker (KKT) conditions that the optimal solution must satisfy

$$\frac{\partial}{\partial \lambda_t^{(i)}} L(\lambda_t, \epsilon_t, \iota) = \epsilon_t^{(i)} - \mu \cdot \frac{1}{\lambda_t^{(i)}} + (\iota^\top F)^{(i)} - \iota_2^{(i)} = 0, \tag{A.1}$$

$$\frac{\partial}{\partial \epsilon_t^{(i)}} L(\lambda_t, \epsilon_t, \iota) = \lambda_t^{(i)} - \mu \cdot \frac{1}{\epsilon_t^{(i)}} - \iota_1^{(i)} - \iota_3^{(i)} = 0, \tag{A.2}$$

$$Dx_t + Eu_t + F\lambda_t + d = \epsilon_t, \tag{A.3}$$

where (A.1), (A.2) follow from the stationarity of the optimal solution, and (A.3) follows from the primal feasibility.

Combining the above equations, we know that $\epsilon_t^{(i)} \lambda_t^{(i)} = \mu$ and $\lambda_t \circ (Dx_t + Eu_t + F\lambda_t + d) = \mu \vec{1}$. □

A.2 Proof of Theorem 4.2

Proof. From the policy update rule, we know that $\widehat{\nabla}_\theta \mathcal{J}(\pi_{\theta_n}) = (\theta_{n+1} - \theta_n)/\eta$. By the Lipschitz Assumption 4.3, we have

$$\begin{aligned}
\mathcal{J}(\pi_{\theta_{n+1}}) - \mathcal{J}(\pi_{\theta_n}) &\geq \nabla_\theta \mathcal{J}(\pi_{\theta_n})^\top (\theta_{n+1} - \theta_n) - \frac{L}{2} \|\theta_{n+1} - \theta_n\|_2^2 \\
&= \eta \nabla_\theta \mathcal{J}(\pi_{\theta_n})^\top \widehat{\nabla}_\theta \mathcal{J}(\pi_{\theta_n}) - \frac{L\eta^2}{2} \big\|\widehat{\nabla}_\theta \mathcal{J}(\pi_{\theta_n})\big\|_2^2.
\end{aligned} \tag{A.4}$$

We rewrite the exact gradient $\nabla_\theta \mathcal{J}(\pi_{\theta_n})$ as

$$\nabla_\theta \mathcal{J}(\pi_{\theta_n}) = \Big(\nabla_\theta \mathcal{J}(\pi_{\theta_n}) - \mathbb{E}\big[\widehat{\nabla}_\theta \mathcal{J}(\pi_{\theta_n})\big]\Big) - \Big(\widehat{\nabla}_\theta \mathcal{J}(\pi_{\theta_n}) - \mathbb{E}\big[\widehat{\nabla}_\theta \mathcal{J}(\pi_{\theta_n})\big]\Big) + \widehat{\nabla}_\theta \mathcal{J}(\pi_{\theta_n}).$$

In order to lower-bound $\nabla_\theta \mathcal{J}(\pi_{\theta_n})^\top \widehat{\nabla}_\theta \mathcal{J}(\pi_{\theta_n})$, we turn to bound the resulting three terms:

$$\begin{aligned}
\left|\Big(\nabla_\theta \mathcal{J}(\pi_{\theta_n}) - \mathbb{E}\big[\widehat{\nabla}_\theta \mathcal{J}(\pi_{\theta_n})\big]\Big)^\top \widehat{\nabla}_\theta \mathcal{J}(\pi_{\theta_n})\right| &\leq \left\|\widehat{\nabla}_\theta \mathcal{J}(\pi_{\theta_n})\right\|_2 \cdot \left\|\nabla_\theta \mathcal{J}(\pi_{\theta_n}) - \mathbb{E}\big[\widehat{\nabla}_\theta \mathcal{J}(\pi_{\theta_n})\big]\right\|_2 \\
&= \left\|\widehat{\nabla}_\theta \mathcal{J}(\pi_{\theta_n})\right\|_2 \cdot b_n, \\
\Big(\widehat{\nabla}_\theta \mathcal{J}(\pi_{\theta_n}) - \mathbb{E}[\widehat{\nabla}_\theta \mathcal{J}(\pi_{\theta_n})]\Big)^\top \widehat{\nabla}_\theta \mathcal{J}(\pi_{\theta_n}) &\leq \frac{\left\|\widehat{\nabla}_\theta \mathcal{J}(\pi_{\theta_n}) - \mathbb{E}\big[\widehat{\nabla}_\theta \mathcal{J}(\pi_{\theta_n})\big]\right\|_2^2}{2} + \frac{\left\|\widehat{\nabla}_\theta \mathcal{J}(\pi_{\theta_n})\right\|_2^2}{2}, \\
\widehat{\nabla}_\theta \mathcal{J}(\pi_{\theta_n})^\top \widehat{\nabla}_\theta \mathcal{J}(\pi_{\theta_n}) &\geq \left\|\widehat{\nabla}_\theta \mathcal{J}(\pi_{\theta_n})\right\|_2^2.
\end{aligned}$$

Thus, we have the following inequality for (A.4):

$$\begin{aligned}
\mathcal{J}(\pi_{\theta_{n+1}}) - \mathcal{J}(\pi_{\theta_n}) \geq \frac{\eta}{2} \cdot \Big(&-\left\|\widehat{\nabla}_\theta \mathcal{J}(\pi_{\theta_n})\right\|_2 \cdot 2b_n - \left\|\widehat{\nabla}_\theta \mathcal{J}(\pi_{\theta_n}) - \mathbb{E}[\widehat{\nabla}_\theta \mathcal{J}(\pi_{\theta_n})]\right\|_2^2 + \left\|\widehat{\nabla}_\theta \mathcal{J}(\pi_{\theta_n})\right\|_2^2\Big) \\
&- \frac{L\eta^2}{2} \cdot \left\|\widehat{\nabla}_\theta \mathcal{J}(\pi_{\theta_n})\right\|_2^2.
\end{aligned} \tag{A.5}$$

By taking expectation in (A.5), we obtain

$$\mathbb{E}[\mathcal{J}(\pi_{\theta_{n+1}}) - \mathcal{J}(\pi_{\theta_n})] \geq -\eta \cdot \mathbb{E}\Big[\big\|\widehat{\nabla}_\theta \mathcal{J}(\pi_{\theta_n})\big\|_2\Big] \cdot b_n - \frac{\eta}{2} \cdot v_n + \frac{\eta - L\eta^2}{2} \cdot \mathbb{E}\Big[\big\|\widehat{\nabla}_\theta \mathcal{J}(\pi_{\theta_n})\big\|_2^2\Big].$$

By rearranging terms,

$$\frac{\eta - L\eta^2}{2} \cdot \mathbb{E}\Big[\big\|\widehat{\nabla}_\theta \mathcal{J}(\pi_{\theta_n})\big\|_2^2\Big] \le \mathbb{E}[\mathcal{J}(\pi_{\theta_{n+1}}) - \mathcal{J}(\pi_{\theta_n})] + \eta \mathbb{E}[\|\widehat{\nabla}_\theta \mathcal{J}(\pi_{\theta_n})\|_2] b_n + \frac{\eta}{2} v_n. \tag{A.6}$$

We now turn our attention to characterize $\|\nabla_\theta \mathcal{J}(\pi_{\theta_n}) - \widehat{\nabla}_\theta \mathcal{J}(\pi_{\theta_n})\|_2$.

$$\begin{aligned}
\mathbb{E}\Big[\big\|\nabla_\theta \mathcal{J}(\pi_{\theta_n}) - \widehat{\nabla}_\theta \mathcal{J}(\pi_{\theta_n})\big\|_2^2\Big] &= \mathbb{E}\Big[\Big\|\nabla_\theta \mathcal{J}(\pi_{\theta_n}) - \mathbb{E}\big[\widehat{\nabla}_\theta \mathcal{J}(\pi_{\theta_n})\big] + \mathbb{E}\big[\widehat{\nabla}_\theta \mathcal{J}(\pi_{\theta_n})\big] - \widehat{\nabla}_\theta \mathcal{J}(\pi_{\theta_n})\Big\|_2^2\Big] \\
&\le 2\Big\|\nabla_\theta \mathcal{J}(\pi_{\theta_n}) - \mathbb{E}\big[\widehat{\nabla}_\theta \mathcal{J}(\pi_{\theta_n})\big]\Big\|_2^2 + 2\mathbb{E}\Big[\Big\|\widehat{\nabla}_\theta \mathcal{J}(\pi_{\theta_n}) - \mathbb{E}\big[\widehat{\nabla}_\theta \mathcal{J}(\pi_{\theta_n})\big]\Big\|_2^2\Big] \\
&= 2b_n^2 + 2v_n,
\end{aligned} \tag{A.7}$$

where the second inequality holds since for any vector $y, z \in \mathbb{R}^d$,

$$\|y + z\|_2^2 \le \|y\|_2^2 + \|z\|_2^2 + 2\|y\|_2 \cdot \|z\|_2 \le 2\|y\|_2^2 + 2\|z\|_2^2. \tag{A.8}$$

Then we are ready to bound the minimum expected gradient norm by relating it to the average norm over T iterations. Specifically,

$$\begin{aligned}
\min_{t\in[T]} \mathbb{E}\Big[\big\|\nabla_\theta \mathcal{J}(\pi_{\theta_n})\big\|_2^2\Big] &\le \frac{1}{N} \cdot \sum_{n=0}^{N-1} \mathbb{E}\Big[\big\|\nabla_\theta \mathcal{J}(\pi_{\theta_n})\big\|_2^2\Big] \\
&\le \frac{2}{N} \cdot \sum_{n=0}^{N-1} \left(\mathbb{E}\left[\|\widehat{\nabla}_\theta \mathcal{J}(\pi_{\theta_n})\|_2^2\right] + \mathbb{E}\Big[\big\|\nabla_\theta \mathcal{J}(\pi_{\theta_n}) - \widehat{\nabla}_\theta \mathcal{J}(\pi_{\theta_n})\big\|_2^2\Big]\right),
\end{aligned}$$

where the second inequality follows from (A.8).

For $N \ge 4L^2$, by setting $\eta = 1/\sqrt{N}$, we have $\eta < 1/L$ and $(\eta - L\eta^2)/2 > 0$. Therefore, following the results in (A.6) and (A.7), we further have

$$\begin{aligned}
&\min_{n\in[N]} \mathbb{E}\Big[\big\|\nabla_\theta \mathcal{J}(\pi_{\theta_n})\big\|_2^2\Big] \\
&\le \frac{4c}{N} \cdot \left(\mathbb{E}[\mathcal{J}(\pi_{\theta_N}) - \mathcal{J}(\pi_{\theta_1})] + \sum_{n=0}^{N-1} \left(\eta \cdot \mathbb{E}\Big[\big\|\widehat{\nabla}_\theta \mathcal{J}(\pi_{\theta_n})\big\|_2\Big] \cdot b_n + \frac{\eta}{2} \cdot v_n\right)\right) + \frac{4}{N} \cdot \sum_{n=0}^{N-1} (b_n^2 + v_n) \\
&= \frac{4}{N} \cdot \left(\sum_{n=0}^{N-1} c \cdot \left(\eta \cdot \mathbb{E}\Big[\big\|\widehat{\nabla}_\theta \mathcal{J}(\pi_{\theta_n})\big\|_2\Big] \cdot b_n + \frac{\eta}{2} \cdot v_n\right) + b_n^2 + v_n\right) + \frac{4c}{N} \cdot \mathbb{E}\big[\mathcal{J}(\pi_{\theta_N}) - \mathcal{J}(\pi_{\theta_1})\big],
\end{aligned}$$

where the last step holds due to the definition $c := \big(\eta - L\eta^2\big)^{-1}$.

By noting that $\eta \widehat{\nabla}_\theta \mathcal{J}(\pi_{\theta_n}) = \theta_{n+1} - \theta_n$, we conclude the proof by

$$\begin{aligned}
&\min_{n\in[N]} \mathbb{E}\Big[\big\|\nabla_\theta \mathcal{J}(\pi_{\theta_n})\big\|_2^2\Big] \\
&\le \frac{4}{N} \cdot \left(\sum_{n=0}^{N-1} c \cdot \left(\mathbb{E}\Big[\big\|\theta_{n+1} - \theta_n\big\|_2\Big] \cdot b_n + \frac{\eta}{2} \cdot v_n\right) + b_n^2 + v_n\right) + \frac{4c}{N} \cdot \mathbb{E}\big[\mathcal{J}(\pi_{\theta_N}) - \mathcal{J}(\pi_{\theta_1})\big] \\
&\le \frac{4}{N} \cdot \left(\sum_{n=0}^{N-1} c \cdot (2\delta \cdot b_n + \frac{\eta}{2} \cdot v_n) + b_n^2 + v_n\right) + \frac{4c}{N} \cdot \mathbb{E}\big[\mathcal{J}(\pi_{\theta_N}) - \mathcal{J}(\pi_{\theta_1})\big].
\end{aligned}$$

where the second inequality holds since $\|\theta\|_2 \le \delta$ for any $\theta \in \Theta$. □

A.3 Proof of Theorem 4.4

In what follows, we interchangeably write $\nabla_a b$ and $\mathrm{d}b/\mathrm{d}a$ as the derivative, and use the notation $\partial b/\partial a$ to denote the partial derivative. With slight abuse of notation, for vector s and vector w, we denote the Jacobian matrix consisting of entries $\partial s^{(i)}/\partial w^{(j)}$ as $\partial s/\partial w$.

Proof. In order to upper-bound the gradient variance $v_n = \mathbb{E}[\|\widehat{\nabla}_\theta \mathcal{J}(\pi_{\theta_n}) - \mathbb{E}[\widehat{\nabla}_\theta \mathcal{J}(\pi_{\theta_n})]\|_2^2]$, we turn to find the supremum of the norm inside the outer expectation, which serves as a loose yet acceptable variance upper bound.

We start with the case when the sample size $M = 1$, which can naturally generalize to $N > 1$. Specifically, consider an *arbitrary* trajectory obtained by unrolling the model under policy π_{θ_n}. Denote the pathwise gradient $\widehat{\nabla}_\theta \mathcal{J}(\pi_{\theta_n})$ of this trajectory as g'. Then we have

$$v_n \leq \max_{g'} \left\| g' - \mathbb{E}\big[\widehat{\nabla}_\theta \mathcal{J}(\pi_{\theta_n})\big] \right\|_2^2 = \left\| g - \mathbb{E}\big[\widehat{\nabla}_\theta \mathcal{J}(\pi_{\theta_n})\big] \right\|_2^2 = \left\| \mathbb{E}\big[g - \widehat{\nabla}_\theta \mathcal{J}(\pi_{\theta_n})\big] \right\|_2^2,$$

where we let g denote the pathwise gradient $\widehat{\nabla}_\theta \mathcal{J}(\pi_{\theta_n})$ of a *fixed* (but unknown) trajectory $(x_0, u_0, x_1, u_1, \cdots)$ such that the maximum is achieved.

Using the fact that $\|\mathbb{E}[\cdot]\|_2 \leq \mathbb{E}[\|\cdot\|_2]$, we further obtain

$$v_n \leq \mathbb{E}\Big[\big\| g - \widehat{\nabla}_\theta \mathcal{J}(\pi_{\theta_n}) \big\|_2 \Big]^2. \tag{A.9}$$

Denote $y_t := (x_t, u_t)$. By triangular inequality, we have

$$\mathbb{E}\Big[\big\| g - \widehat{\nabla}_\theta \mathcal{J}(\pi_{\theta_n}) \big\|_2 \Big] \leq \sum_{t=0}^{H-1} \mathbb{E}_{\overline{y}_t} \Big[\big\| \nabla_\theta r(y_t) - \nabla_\theta r(\overline{y}_t) \big\|_2 \Big]. \tag{A.10}$$

For $t \geq 1$, we have the following relationship according to the chain rule:

$$\frac{\mathrm{d}u_t}{\mathrm{d}\theta} = \frac{\partial u_t}{\partial x_t} \cdot \frac{\mathrm{d}x_t}{\mathrm{d}\theta} + \frac{\partial u_t}{\partial \theta}, \tag{A.11}$$

$$\frac{\mathrm{d}x_t}{\mathrm{d}\theta} = \frac{\partial x_t}{\partial x_{t-1}} \cdot \frac{\mathrm{d}x_{t-1}}{\mathrm{d}\theta} + \frac{\partial x_t}{\partial u_{t-1}} \cdot \frac{\mathrm{d}u_{t-1}}{\mathrm{d}\theta}. \tag{A.12}$$

Plugging $\mathrm{d}u_{t-1}/\mathrm{d}\theta$ in (A.11) into (A.12), we get

$$\frac{\mathrm{d}x_t}{\mathrm{d}\theta} = \left(\frac{\partial x_t}{\partial x_{t-1}} + \frac{\partial x_t}{\partial u_{t-1}} \cdot \frac{\partial u_{t-1}}{\partial x_{t-1}} \right) \cdot \frac{\mathrm{d}x_{t-1}}{\mathrm{d}\theta} + \frac{\partial x_t}{\partial u_{t-1}} \cdot \frac{\partial u_{t-1}}{\partial \theta}. \tag{A.13}$$

By the Cauchy-Schwarz inequality and the Lipschitz Assumption 4.3, we have

$$\left\| \frac{\mathrm{d}x_t}{\mathrm{d}\theta} \right\|_2 \leq L_f \widetilde{L}_\pi \cdot \left\| \frac{\mathrm{d}x_{t-1}}{\mathrm{d}\theta} \right\|_2 + L_f L_\theta.$$

Applying the above recursion gives us

$$\left\| \frac{\mathrm{d}x_t}{\mathrm{d}\theta} \right\|_2 \leq L_f L_\theta \cdot \sum_{j=0}^{t-1} L_f^j \widetilde{L}_\pi^j \leq i \cdot L_\theta L_f^{t+1} \widetilde{L}_\pi^t, \tag{A.14}$$

where the first inequality follows from the induction

$$z_n = a z_{t-1} + b = a \cdot (a z_{i-2} + b) + b = a^t \cdot z_0 + b \cdot \sum_{j=0}^{t-1} a^j, \tag{A.15}$$

for the real sequence $\{z_j\}_{0 \leq j \leq i}$ satisfying $z_j = a z_{j-1} + b$. For $\mathrm{d}u_t/\mathrm{d}\theta$ defined in (A.11), we further have

$$\left\| \frac{\mathrm{d}u_t}{\mathrm{d}\theta} \right\|_2 \leq L_\pi \cdot \left\| \frac{\mathrm{d}x_t}{\mathrm{d}\theta} \right\|_2 + L_\theta \leq t \cdot L_\theta L_f^{t+1} \widetilde{L}_\pi^{t+1} + L_\theta. \tag{A.16}$$

Combining (A.14) and (A.16), we obtain

$$\left\| \frac{\mathrm{d}y_t}{\mathrm{d}\theta} \right\|_2 = \left\| \frac{\mathrm{d}x_t}{\mathrm{d}\theta} \right\|_2 + \left\| \frac{\mathrm{d}u_t}{\mathrm{d}\theta} \right\|_2 \leq K(t) := 2t \cdot L_\theta L_f^{t+1} \widetilde{L}_\pi^{t+1} + L_\theta, \tag{A.17}$$

where $K(t)$ is introduced for notation simplicity.

By the chain rule, (A.10) can be decomposed and bounded by

$$\begin{aligned}
&\mathbb{E}_{\overline{y}_t}\left[\left\|\nabla_\theta r(y_t) - \nabla_\theta r(\overline{y}_t)\right\|_2\right] \\
&= \mathbb{E}_{\overline{y}_t}\left[\left\|\nabla r(y_t)\nabla_\theta y_t - \nabla r(\overline{y}_t)\nabla_\theta \overline{y}_t\right\|_2\right] \\
&\le \mathbb{E}_{\overline{y}_t}\left[\left\|\nabla r(y_t)\nabla_\theta y_t - \nabla r(y_t)\nabla_\theta \overline{y}_t\right\|_2\right] + \mathbb{E}\left[\left\|\nabla r(y_t)\nabla_\theta \overline{y}_t - \nabla r(\overline{y}_t)\nabla_\theta \overline{y}_t\right\|_2\right] \\
&\le L_r \cdot \left(\mathbb{E}_{\overline{x}_n}\left[\left\|\frac{\mathrm{d}x_t}{\mathrm{d}\theta} - \frac{\mathrm{d}\overline{x}_t}{\mathrm{d}\theta}\right\|_2\right] + \mathbb{E}_{\overline{u}_n}\left[\left\|\frac{\mathrm{d}u_t}{\mathrm{d}\theta} - \frac{\mathrm{d}\overline{u}_t}{\mathrm{d}\theta}\right\|_2\right]\right) + 2L_r \cdot K(t),
\end{aligned} \tag{A.18}$$

where the last step follows from the Cauchy-Schwartz inequality and the Lipschitz reward assumption.

Plugging (A.18) into (A.10) and (A.9), we have

$$\begin{aligned}
v_n &\le L_r \cdot \left(\sum_{t=0}^{H-1}\left(\mathbb{E}_{\overline{x}_t}\left[\left\|\frac{\mathrm{d}x_t}{\mathrm{d}\theta} - \frac{\mathrm{d}\overline{x}_t}{\mathrm{d}\theta}\right\|_2\right] + \mathbb{E}_{\overline{u}_t}\left[\left\|\frac{\mathrm{d}u_t}{\mathrm{d}\theta} - \frac{\mathrm{d}\overline{u}_t}{\mathrm{d}\theta}\right\|_2\right] + 2K(t)\right)\right)^2 \\
&\le O\left(\left(\sum_{t=0}^{H-1} t^2 \widetilde{L}_f^{2t}\widetilde{L}_\pi^{2t}\right)^2\right) = O\left(H^4 \widetilde{L}_f^{4H}\widetilde{L}_\pi^{4H}\right),
\end{aligned} \tag{A.19}$$

where the second inequality follows from the results from Lemma A.1 and by plugging the definition of K in (A.17). Since the analysis above considers batch size $M = 1$, the bound of gradient variance v_n is established by dividing M, which concludes the proof. □

Lemma A.1. Denote $e := \sup \mathbb{E}_{\overline{x}_0}[\|\mathrm{d}x_0/\mathrm{d}\theta - \mathrm{d}\overline{x}_0/\mathrm{d}\theta\|_2]$, which is a constant that only depends on the initial state distribution[1]. For any timestep $t \ge 1$ and the corresponding state x_t, control input u_t, we have the following inequality results:

$$\begin{aligned}
\mathbb{E}_{\overline{x}_t}\left[\left\|\frac{\mathrm{d}x_t}{\mathrm{d}\theta} - \frac{\mathrm{d}\overline{x}_t}{\mathrm{d}\theta}\right\|_2\right] &\le \widetilde{L}_f^t\widetilde{L}_\pi^t\left(e + 4t \cdot \widetilde{L}_f\widetilde{L}_\pi \cdot K(t-1) + 2t \cdot \widetilde{L}_f L_\theta\right), \\
\mathbb{E}_{\overline{u}_n}\left[\left\|\frac{\mathrm{d}u_t}{\mathrm{d}\theta} - \frac{\mathrm{d}\overline{u}_t}{\mathrm{d}\theta}\right\|_2\right] &\le \widetilde{L}_f^t\widetilde{L}_\pi^{t+1}\left(e + 4i \cdot \widetilde{L}_f\widetilde{L}_\pi \cdot K(t-1) + 2t \cdot \widetilde{L}_f L_\theta\right) + 2L_\pi K(t) + 2L_\theta.
\end{aligned}$$

Proof. Firstly, we obtain from (A.12) that $\forall t \ge 1$,

$$\begin{aligned}
&\mathbb{E}_{\overline{x}_t}\left[\left\|\frac{\mathrm{d}x_t}{\mathrm{d}\theta} - \frac{\mathrm{d}\overline{x}_t}{\mathrm{d}\theta}\right\|_2\right] \\
&= \mathbb{E}\left[\left\|\frac{\partial x_t}{\partial x_{t-1}} \cdot \frac{\mathrm{d}x_{t-1}}{\mathrm{d}\theta} + \frac{\partial x_t}{\partial u_{t-1}} \cdot \frac{\mathrm{d}u_{t-1}}{\mathrm{d}\theta} - \frac{\partial \overline{x}_t}{\partial \overline{x}_{t-1}} \cdot \frac{\mathrm{d}\overline{x}_{t-1}}{\mathrm{d}\theta} - \frac{\partial \overline{x}_t}{\partial \overline{u}_{t-1}} \cdot \frac{\mathrm{d}\overline{u}_{t-1}}{\mathrm{d}\theta}\right\|_2\right]
\end{aligned}$$

According to the triangle inequality, we continue with

$$\begin{aligned}
&\le \mathbb{E}\left[\left\|\frac{\partial x_t}{\partial x_{t-1}} \cdot \frac{\mathrm{d}x_{t-1}}{\mathrm{d}\theta} - \frac{\partial \overline{x}_t}{\partial \overline{x}_{t-1}} \cdot \frac{\mathrm{d}x_{t-1}}{\mathrm{d}\theta}\right\|_2\right] + \mathbb{E}\left[\left\|\frac{\partial \overline{x}_t}{\partial \overline{x}_{t-1}} \cdot \frac{\mathrm{d}x_{t-1}}{\mathrm{d}\theta} - \frac{\partial \overline{x}_t}{\partial \overline{x}_{t-1}} \cdot \frac{\mathrm{d}\overline{x}_{t-1}}{\mathrm{d}\theta}\right\|_2\right] \\
&\quad + \mathbb{E}\left[\left\|\frac{\partial x_t}{\partial u_{t-1}} \cdot \frac{\mathrm{d}u_{t-1}}{\mathrm{d}\theta} - \frac{\partial \overline{x}_t}{\partial \overline{u}_{t-1}} \cdot \frac{\mathrm{d}u_{t-1}}{\mathrm{d}\theta}\right\|_2\right] + \mathbb{E}\left[\left\|\frac{\partial \overline{x}_t}{\partial \overline{u}_{t-1}} \cdot \frac{\mathrm{d}u_{t-1}}{\mathrm{d}\theta} - \frac{\partial \overline{x}_t}{\partial \overline{u}_{t-1}} \cdot \frac{\mathrm{d}\overline{u}_{t-1}}{\mathrm{d}\theta}\right\|_2\right] \\
&\le 2L_f \cdot \left(\left\|\frac{\mathrm{d}x_{t-1}}{\mathrm{d}\theta}\right\|_2 + \left\|\frac{\mathrm{d}u_{t-1}}{\mathrm{d}\theta}\right\|_2\right) + L_f \cdot \mathbb{E}_{\overline{x}_{t-1}}\left[\left\|\frac{\mathrm{d}x_{t-1}}{\mathrm{d}\theta} - \frac{\mathrm{d}\overline{x}_{t-1}}{\mathrm{d}\theta}\right\|_2\right] \\
&\quad + L_f \cdot \mathbb{E}_{\overline{u}_{t-1}}\left[\left\|\frac{\mathrm{d}u_{t-1}}{\mathrm{d}\theta} - \frac{\mathrm{d}\overline{u}_{t-1}}{\mathrm{d}\theta}\right\|_2\right].
\end{aligned} \tag{A.20}$$

[1] We define e to account for the stochasticity of the initial state distribution. $e = 0$ when the initial state is deterministic.

Similarly, we have from (A.11) that

$$\begin{aligned}
&\mathbb{E}_{\overline{u}_n}\left[\left\|\frac{\mathrm{d}u_t}{\mathrm{d}\theta}-\frac{\mathrm{d}\overline{u}_t}{\mathrm{d}\theta}\right\|_2\right] \\
&\quad=\mathbb{E}\left[\left\|\frac{\partial u_t}{\partial x_t}\cdot\frac{\mathrm{d}x_t}{\mathrm{d}\theta}+\frac{\partial u_t}{\partial\theta}-\frac{\partial\overline{u}_t}{\partial\overline{x}_t}\cdot\frac{\mathrm{d}\overline{x}_t}{\mathrm{d}\theta}-\frac{\partial\overline{u}_t}{\partial\theta}\right\|_2\right] \\
&\quad\le\mathbb{E}\left[\left\|\frac{\partial u_t}{\partial x_t}\cdot\frac{\mathrm{d}x_t}{\mathrm{d}\theta}-\frac{\partial\overline{u}_t}{\partial\overline{x}_t}\cdot\frac{\mathrm{d}x_t}{\mathrm{d}\theta}\right\|_2\right]+\mathbb{E}\left[\left\|\frac{\partial\overline{u}_t}{\partial\overline{x}_t}\cdot\frac{\mathrm{d}x_t}{\mathrm{d}\theta}-\frac{\partial\overline{u}_t}{\partial\overline{x}_t}\cdot\frac{\mathrm{d}\overline{x}_t}{\mathrm{d}\theta}\right\|_2\right]+\mathbb{E}\left[\left\|\frac{\partial u_t}{\partial\theta}-\frac{\partial\overline{u}_t}{\partial\theta}\right\|_2\right] \\
&\quad\le 2L_\pi\cdot\mathbb{E}\left[\left\|\frac{\mathrm{d}x_t}{\mathrm{d}\theta}\right\|\right]+L_\pi\cdot\mathbb{E}\left[\left\|\frac{\mathrm{d}x_t}{\mathrm{d}\theta}-\frac{\mathrm{d}\overline{x}_t}{\mathrm{d}\theta}\right\|_2\right]+2L_\theta. \qquad \text{(A.21)}
\end{aligned}$$

Plugging (A.21) back to (A.20),

$$\begin{aligned}
&\mathbb{E}_{\overline{x}_t}\left[\left\|\frac{\mathrm{d}x_t}{\mathrm{d}\theta}-\frac{\mathrm{d}\overline{x}_t}{\mathrm{d}\theta}\right\|_2\right] \\
&\quad\lesssim 4L_f\widetilde{L}_\pi\cdot\left(\left\|\frac{\mathrm{d}x_{t-1}}{\mathrm{d}\theta}\right\|_2+\left\|\frac{\mathrm{d}u_{t-1}}{\mathrm{d}\theta}\right\|_2\right)+L_f\widetilde{L}_\pi\cdot\mathbb{E}_{\overline{x}_{t-1}}\left[\left\|\frac{\mathrm{d}x_{t-1}}{\mathrm{d}\theta}-\frac{\mathrm{d}\overline{x}_{t-1}}{\mathrm{d}\theta}\right\|_2\right]+2L_fL_\theta \\
&\quad\le 4L_f\widetilde{L}_\pi\cdot K(t-1)+L_f\widetilde{L}_\pi\cdot\mathbb{E}_{\overline{x}_{t-1}}\left[\left\|\frac{\mathrm{d}x_{t-1}}{\mathrm{d}\theta}-\frac{\mathrm{d}\overline{x}_{t-1}}{\mathrm{d}\theta}\right\|_2\right]+2L_fL_\theta,
\end{aligned}$$

where the last inequality follows from the definition of K in (A.17).

Applying this recursion gives us

$$\begin{aligned}
\mathbb{E}_{\overline{x}_t}\left[\left\|\frac{\mathrm{d}x_t}{\mathrm{d}\theta}-\frac{\mathrm{d}\overline{x}_t}{\mathrm{d}\theta}\right\|_2\right]&=e\big(L_f\widetilde{L}_\pi\big)^t+\big(4L_f\widetilde{L}_\pi\cdot K(t-1)+2\widetilde{L}_fL_\theta\big)\cdot\sum_{j=0}^{t-1}\big(\widetilde{L}_f\widetilde{L}_\pi\big)^j \\
&\le\widetilde{L}_f^t\widetilde{L}_\pi^t\Big(e+4t\cdot\widetilde{L}_f\widetilde{L}_\pi\cdot K(t-1)+2t\cdot\widetilde{L}_fL_\theta\Big),
\end{aligned}$$

where the first equality follows from (A.15).

As a consequence, we have from (A.21) that

$$\mathbb{E}_{\overline{u}_t}\left[\left\|\frac{\mathrm{d}u_t}{\mathrm{d}\theta}-\frac{\mathrm{d}\overline{u}_t}{\mathrm{d}\theta}\right\|_2\right]\le\widetilde{L}_f^t\widetilde{L}_\pi^{t+1}\Big(e+4t\cdot\widetilde{L}_f\widetilde{L}_\pi\cdot K(t-1)+2t\cdot\widetilde{L}_fL_\theta\Big)+2L_\pi K(t)+2L_\theta.$$

This concludes the proof. □

A.4 Proof of Theorem 4.5

In the following proof, we use the notation $\|z\|_2$ to represent the Euclidean l_2 norm for vector z, and $\|Z\|_2$ to represent the induced 2-norm for matrix Z, i.e. $\|Z\|_2:=\max_{\|x\|_2=1}\|Zx\|_2$. Recall that $\|Z\|_F$ denotes the Frobenius norm of matrix Z, i.e. $\|Z\|_F=\sqrt{\mathrm{tr}(ZZ^\top)}$.

To characterize the Lipschitz of the LCS model, we need the partial derivatives of x_{t+1} with respect to x_t and u_t, which, however, further depend on the partial derivatives of λ_t with respect to x_t and u_t and cannot be expressed in closed form. Instead, they are implicitly defined by the LCP. Therefore, we introduce the following implicit function theorem.

Theorem A.2 (Implicit Function Theorem)**.** An implicit function $g:\mathbb{R}^{d_s}\times\mathbb{R}^{d_w}\to\mathbb{R}^{d_s}$ is defined as $g(s,w)=0$ for solution $s\in\mathbb{R}^{d_s}$ and problem data $w\in\mathbb{R}^{d_w}$. Then the Jacobian $\partial s/\partial w$, i.e. the sensitivity of the solution with respect to the problem data, is given by

$$\frac{\partial s}{\partial w}=-\Big(\frac{\partial g}{\partial s}\Big)^{-1}\frac{\partial g}{\partial w}.$$

Proof. Differentiating g with respect to the problem data w gives:

$$\frac{\mathrm{d}g}{\mathrm{d}w}=\frac{\partial g}{\partial w}+\frac{\partial g}{\partial s}\frac{\partial s}{\partial w}.$$

Since for any w, $g(s,w)=0$ always holds, the above total derivative is also always 0. This observation allows us to calculate the Jacobian

$$\frac{\partial s}{\partial w} = -\Big(\frac{\partial g}{\partial s}\Big)^{-1}\frac{\partial g}{\partial w}.$$

□

Proof of Theorem 4.5. To begin with, we first study the Jacobian $\partial x_{t+1}/\partial x_t$, and the Jacobian $\partial x_{t+1}/\partial u_t$ can be analyzed using similar techniques.

Denote $C^{(i)} \in \mathbb{R}^{d_x}$ as the i-th column of the matrix $C \in \mathbb{R}^{d_x \times d_\lambda}$. Similarly, denote $D^{(i)} \in \mathbb{R}^{d_x}$, $E^{(i)} \in \mathbb{R}^{d_u}$, $F^{(i)} \in \mathbb{R}^{d_\lambda}$ as the i-the rows of matrices D, E, F, respectively. Then we have the Jacobian with the form

$$\frac{\partial x_{t+1}}{\partial x_t} = A + \sum_{i=1}^{d_\lambda} C^{(i)} \frac{\partial \lambda^{(i)}}{\partial x_t}. \tag{A.22}$$

We rewrite the contact equation $\lambda_t \circ (Dx_t + Eu_t + F\lambda_t + d) = \mu \vec{1}$ in (3.1) as

$$\lambda_t^{(i)}(D^{(i)\top}x_t + E^{(i)\top}u_t + F^{(i)\top}\lambda_t + d^{(i)}) = \mu, \ \ \forall i \in [1, d_\lambda]. \tag{A.23}$$

By the Implicit Function Theorem A.2, we have

$$\begin{aligned}\frac{\partial \lambda^{(i)}}{\partial x_t} &= -\Big(D^{(i)\top}x_t + E^{(i)\top}u_t + \frac{\partial}{\partial \lambda_t^{(i)}}\lambda_t^{(i)}F^{(i)\top}\lambda_t + d^{(i)}\Big)^{-1}\lambda_t^{(i)}D^{(i)\top} \\ &= -(D^{(i)\top}x_t + E^{(i)\top}u_t + F^{(i)\top}\lambda_t + \lambda_t^{(i)}F^{(i)(i)} + d^{(i)})^{-1}\lambda_t^{(i)}D^{(i)\top}, \ \ \forall i \in [1, d_\lambda],\end{aligned} \tag{A.24}$$

where $F^{(i)(i)} \in \mathbb{R}$ is the i-th element of $F^{(i)}$.

Since F is a P-matrix, we know that all its first order principal sub-matrices are positive, i.e., $F^{(i)(i)} > 0$.

Plugging (A.24) into (A.22) and take the induced 2-norm, we obtain

$$\begin{aligned}\left\|\frac{\partial x_{t+1}}{\partial x_t}\right\|_2 &= \left\|A - \sum_{i=1}^{d_\lambda} C^{(i)}\big(D^{(i)\top}x_t + E^{(i)\top}u_t + F^{(i)\top}\lambda_t + \lambda_t^{(i)}F^{(i)(i)} + d^{(i)}\big)^{-1}\lambda_t^{(i)}D^{(i)\top}\right\|_2 \\ &\le \|A\|_2 + \sum_{i=1}^{d_\lambda} \lambda_t^{(i)}\|C^{(i)}\|_2 \cdot \|D^{(i)}\|_2 \cdot \big|D^{(i)\top}x_t + E^{(i)\top}u_t + F^{(i)\top}\lambda_t + \lambda_t^{(i)}F^{(i)(i)} + d^{(i)}\big|^{-1} \\ &\le \|A\|_2 + \sum_{i=1}^{d_\lambda} \|C^{(i)}\|_2 \cdot \|D^{(i)}\|_2 \cdot (\lambda_t^{(i)})^2/\mu,\end{aligned} \tag{A.25}$$

where the first inequality holds due to the Cauchy–Schwarz inequality, the second inequality holds since $F^{(i)(i)} > 0$ and $D^{(i)\top}x_t + E^{(i)\top}u_t + F^{(i)\top}\lambda_t + d^{(i)} \ge 0$.

By the definition of Frobenius norm, we know that

$$\begin{aligned}\|C\|_F &= \sqrt{\sum_{i=1}^{d_\lambda}\|C^{(i)}\|_2^2} = \sqrt{d_\lambda}\cdot\sqrt{\sum_{i=1}^{d_\lambda}\frac{1}{d_\lambda}\|C^{(i)}\|_2^2} \\ &\ge \sqrt{d_\lambda}\cdot\sum_{i=1}^{d_\lambda}\frac{1}{d_\lambda}\sqrt{\|C^{(i)}\|_2^2} = \frac{1}{\sqrt{d_\lambda}}\sum_{i=1}^{d_\lambda}\|C^{(i)}\|_2,\end{aligned} \tag{A.26}$$

where we adopt the Jensen's inequality in the second line.

Besides, define the diagonal matrix $\Lambda_t := \mathrm{diag}(\lambda_t^{(1)}, \cdots, \lambda_t^{(d_\lambda)}) \in \mathbb{R}^{d_\lambda \times d_\lambda}$. By definition, $\|\Lambda_t\|_2 = \max_i \lambda^{(i)}$ and thus

$$\|\lambda_t\|_2^2 = \sum_{i=1}^{d_\lambda}(\lambda_t^{(i)})^2 \le d_\lambda \cdot \|\Lambda_t\|_F^2. \tag{A.27}$$

Therefore, we can further bound (A.25) by

$$\begin{aligned}\left\|\frac{\partial x_{t+1}}{\partial x_t}\right\|_2 &\leq \|A\|_2 + \frac{1}{\mu}\left(\sum_{i=1}^{d_\lambda}\|C^{(i)}\|_2\right)\cdot\left(\sum_{i=1}^{d_\lambda}\|D^{(i)}\|_2\right)\cdot\left(\sum_{i=1}^{d_\lambda}(\lambda_t^{(i)})^2\right)\\ &\leq \|A\|_2 + \frac{d_\lambda}{\mu}\|C\|_F\|D\|_F\|\lambda_t\|_2^2\\ &\leq \|A\|_F + \frac{d_\lambda^2}{\mu}\|C\|_F\|D\|_F\|\Lambda_t\|_F^2, \end{aligned} \tag{A.28}$$

where the first inequality holds since $\sum_i y_i \cdot z_i \leq (\sum_i y_i)\cdot(\sum_i z_i)$ for any non-negative scalar sequences y_i, z_i and the second inequality follows from (A.26). The third inequality follows from (A.27) and the fact that $\|A\|_2 \leq \|A\|_F$.

The final step is to characterize the magnitude of $\|\Lambda_t\|_F^2$. This can be done by rewriting the contact equation $\lambda_t \circ (Dx_t + Eu_t + F\lambda_t + d) = \mu\vec{1}$ in (3.1) as

$$\Lambda_t(Dx_t + Eu_t + F\Lambda_t\vec{1} + d) = \mu\vec{1}$$

By the Cauchy-Schwartz inequality we have

$$\|\Lambda_t\|_F \cdot \left(\|Dx_t + Eu_t + d\|_2 + \|F\|_F\|\Lambda_t\|_F\right) \geq \mu.$$

Denote $e := \sup\|Dx_t + Eu_t + d\|_2$. The above inequality can be simplified as

$$\|F\|_F \cdot \|\Lambda_t\|_F^2 + e\cdot\|\Lambda_t\|_F - \mu \geq 0. \tag{A.29}$$

Solving (A.29) gives

$$\|\Lambda_t\|_F \geq \frac{\sqrt{e^2 + 4\mu\|F\|_F} - e}{2\|F\|_F}$$

Since $\varepsilon = e^2/(2\|F\|_F^2)$, we further have

$$\begin{aligned} l(\mu) :=& \frac{\|\Lambda_t\|_F^2}{\mu} \geq \frac{2e^2 + 4\mu\|F\|_F - 2e\sqrt{e^2 + 4\mu\|F\|_F}}{4\mu\|F\|_F^2}\\ =& \frac{e^2}{2\mu\|F\|_F^2} + \frac{1}{\|F\|_F} + \frac{e^2\sqrt{\frac{1}{\mu^2} + \frac{4\|F\|_F}{\mu e^2}}}{2\|F\|_F^2}\\ =& \frac{\varepsilon}{\mu} + \frac{1}{\|F\|_F} + \varepsilon\sqrt{\frac{1}{\mu^2} + \frac{2}{\varepsilon\mu\|F\|_F}}. \end{aligned} \tag{A.30}$$

Plug (A.30) into (A.28), we get the Jacobian norm

$$\left\|\frac{\partial x_{t+1}}{\partial x_t}\right\|_2 \leq \|A\|_F + d_\lambda^2\|C\|_F\|D\|_F\cdot l(\mu).$$

Using the same proof steps, the norm of Jacobian $\partial x_{t+1}/\partial u_t$ satisfies

$$\left\|\frac{\partial x_{t+1}}{\partial u_t}\right\|_2 \leq \|B\|_F + d_\lambda^2\|C\|_F\|E\|_F\cdot l(\mu).$$

We conclude the proof by noticing the relationship between the norm of Jacobian and the Lipschitz of the LCS model. □

A.5 Proof of Proposition 5.1

Proof. We first consider the original unsmoothed problem $\lambda_t(Dx_t + Eu_t + F\lambda_t + d) = 0$. Since $\lambda_t \geq 0$, we know that the solution λ_t is a piece-wise linear function with the form:

$$\lambda_t = \begin{cases} -(Dx_t + Eu_t + d)/F & \text{if } Dx_t + Eu_t + d \leq 0\\ 0 & \text{else} \end{cases}.$$

By rewriting the above function as a function of $z_t := Dx_t + Eu_t + d$, we can express the solver $S_{\mu=0}$ of the exact LCP as follows:

$$S_{\mu=0}(z_t) = \begin{cases} -z_t/F & \text{if } z_t \leq 0 \\ 0 & \text{else} \end{cases}. \tag{A.31}$$

Now our goal is to find the noise distribution $\rho(w)$ such that the following holds:

$$S_{\mu(z_t)}(z_t) = \mathbb{E}_{w\sim\rho(w)}[S_{\mu=0}(z_t + w)] = \int S_{\mu=0}(z_t + w)\rho(w)\mathrm{d}w. \tag{A.32}$$

Define H(x) as a Heaviside-like step function:

$$H(x) := \begin{cases} -1/F & \text{if } x \leq 0 \\ 0 & \text{else} \end{cases}.$$

We observe that the derivative of $S_{\mu=0}(z_t)$ is in fact $H(z_t)$. This allows us to write

$$\begin{aligned} \nabla_{z_t} S_{\mu(z_t)}(z_t) &= \nabla_{z_t} \int S_{\mu=0}(z_t + w)\rho(w)\mathrm{d}w \\ &= \int \nabla_{z_t} S_{\mu=0}(z_t + w)\rho(w)\mathrm{d}w \\ &= \int H(z_t + w)\rho(w)\mathrm{d}w. \end{aligned}$$

Since the derivative of the Heaviside step function is the dirac delta function $\delta(\cdot)$, we have

$$\begin{aligned} \nabla^2_{z_t} S_{\mu(z_t)}(z_t) &= \nabla_{z_t} \int H(z_t + w)\rho(w)\mathrm{d}w \\ &= \int \delta(z_t + w)\rho(w)\mathrm{d}w = \rho(z_t). \end{aligned}$$

This concludes the proof. □

A.6 Proof of Proposition 5.2

Recall that Proposition 5.1 connects the proposed analytic barrier smoothing with the randomized smoothing. Therefore, we first provide the following lemma established in randomized smoothing as a preparation before proving Proposition 5.2.

Lemma A.3 (Randomized Smoothing as Linearization Minimizer (Pang et al., 2022))**.** Let $\rho(w) = \mathcal{N}(0, \Sigma)$ be a zero-mean, Σ-covariance Gaussian. Consider the problem of regressing a function g with parameters (K, W) such that the residual around $\overline{x}$ distributed according to ρ is minimized:

$$\mathcal{L}(K, W) = \min_{K,W} \frac{1}{2}\mathbb{E}_{w\sim\rho(w)}\left[\left\|g(\overline{x} + w) - Ww - K\right\|_2^2\right]. \tag{A.33}$$

The solution is the linearization of the smoothed surrogate:

$$\begin{aligned} K^* &= \mathbb{E}_{w\sim\rho(w)}[g(\overline{x} + w)], \\ W^* &= \frac{\partial}{\partial x}\mathbb{E}_{w\sim\rho(w)}[g(x + w)]|_{x=\overline{x}}. \end{aligned}$$

Proof. The proof is originally provided in (Pang et al., 2022). We adapt it here for completeness.

Since (A.33) is a linear regression problem and is convex, the first-order stationarity condition implies optimality. By calculating the gradients and setting them to zero, we have

$$\begin{aligned} \frac{\partial \mathcal{L}}{\partial K} &= \mathbb{E}_{w\sim\rho(w)}[g(\overline{x} + w)] - K^* = 0 \\ \frac{\partial \mathcal{L}}{\partial W} &= \mathbb{E}_{w\sim\rho(w)}[ww^\top]W^* - \mathbb{E}_{w\sim\rho(w)}[g(\overline{x} + w)w^\top] = 0. \end{aligned}$$

Therefore, we obtain the solution

$$\begin{aligned} K^* &= \mathbb{E}_{w\sim\rho(w)}[g(\overline{x}+w)], \\ W^* &= \mathbb{E}_{w\sim\rho(w)}[ww^\top]^{-1}\mathbb{E}_{w\sim\rho(w)}[g(\overline{x}+w)w^\top] \\ &= \frac{\partial}{\partial x}\mathbb{E}_{w\sim\rho(w)}[g(x+w)]|_{x=\overline{x}}, \end{aligned} \tag{A.34}$$

where the last step follows from the likelihood ratio gradient with the form (2.1), as well as the fact that the score function of the Gaussian is $\Sigma^{-1}w$. □

Proof of Proposition 5.2. By applying Lemma A.3, we know that Proposition 5.2 holds once the following equivalence is established:

$$S_{\mu(z_t)}(z_t) = \mathbb{E}_{w\sim\rho(w)}[S_{\mu=0}(z_t+w)], \tag{A.35}$$

where $\rho(w)$ is any zero-mean Gaussian distribution.

This is a direct result from Proposition 5.1. Specifically, when $\mu(z_t) = \kappa\cdot(z_t+F\kappa)$, the corresponding softened LCP is

$$\lambda_t(z_t+F\lambda_t) = \mu(z_t) = \kappa\cdot(z_t+F\kappa).$$

The solution of the above equation is given by

$$S_{\mu(z_t)}(z_t) = \lambda_t = \kappa = z_t\cdot\mathrm{erf}(z_t,\sigma) + e^{-z_t^2/(2\sigma)}/\sqrt{\pi} + c_1 z_t + c_2. \tag{A.36}$$

Proposition 5.1 states that when $\rho(w) = \nabla_w^2 S_{\mu(z_t)}(w)$, then $S_{\mu(z_t)}(z_t) = \mathbb{E}_{w\sim\rho(w)}[S_{\mu=0}(z_t+w)]$. For $S_{\mu(z_t)}(z_t)$ satisfying (A.36), its second-order derivative is the Gaussian $\mathcal{N}(0,\sigma)$, due to the definition of the error function. Therefore, $S_{\mu(z_t)}(z_t) = \mathbb{E}_{w\sim\mathcal{N}(w;0,\sigma)}[S_{\mu=0}(z_t+w)]$, which concludes the proof of (A.35) and the proposition. □

A.7 Proof of Theorem 5.3

Proof. According to Taylor's theorem, we know that

$$\left|\frac{S_{\mu=0}(z_r+w)-S_{\mu=0}(z_t)}{w} - \nabla_z S_{\mu=0}(z_t)\right| \le |w|\cdot\sup\frac{|\nabla_z^2 S_{\mu=0}(z_t)|}{2} = \frac{F^2|w|}{2}, \tag{A.37}$$

where the second inequality follows from (A.31).

We define the linearization residual at point z_t+w as

$$\nu(w) := \left|S_{\mu=0}(z_r+w) - \nabla_z S_{\mu(z_t)}(z_t)\cdot w - S_{\mu(z_t)}(z_t)\right|.$$

Then we have from (A.37) that

$$\left|\frac{\nu(w)+S_{\mu(z_t)}(z_t)-S_{\mu=0}(z_t)}{w} + \nabla_z S_{\mu(z_t)}(z_t) - \nabla_z S_{\mu=0}(z_t)\right| \le \frac{F^2|w|}{2}.$$

Since $|S_{\mu(z_t)}(z_t) - S_{\mu=0}(z_t)| \le 1/\sqrt{\pi}+c_2 := \varsigma$, achieved at $z=0$, we obtain from the triangle inequality that the bias of gradient satisfies

$$\left|\nabla_z S_{\mu(z_t)}(z_t) - \nabla_z S_{\mu=0}(z_t)\right| \le \frac{F^2|w|}{2} + \frac{\nu(w)+\varsigma}{|w|}. \tag{A.38}$$

From Proposition 5.2, we know that

$$\mathbb{E}_{w\sim\mathcal{N}(0,\sigma)}[\nu(w)] = \delta. \tag{A.39}$$

We claim that there exists $\sigma\mathcal{Q}(2/3) \le w \le \sigma\mathcal{Q}(3/4)$ such that $\nu(w) \le 12\delta$.

This can be proved by contradiction: Suppose $\forall w \in [\sigma\mathcal{Q}(2/3), \sigma\mathcal{Q}(3/4)]$, $\nu(w) > 12\delta$. Then the expectation $\mathbb{E}_{w\sim\mathcal{N}(0,\sigma)}[\nu(w)] > (3/4-2/3)\cdot 12\delta = \delta$. This contradicts with (A.39). Therefore, the claim is correct.

Using the above claim, we have from (A.38) that

$$\left|\nabla_z S_{\mu(z_t)}(z_t) - \nabla_z S_{\mu=0}(z_t)\right| \leq \frac{F^2\sigma\mathcal{Q}(3/4)}{2} + \frac{12\delta+\varsigma}{\sigma\mathcal{Q}(2/3)}.$$

We conclude the proof by applying chain rule in the LCS model (3.1):

$$\left\|\nabla_x f_{\mu=0} - \nabla_x f_{\mu(z_t)}\right\|_2 \leq \|C\|_F\|D\|_F \cdot \left(\frac{\sigma F^2\mathcal{Q}(3/4)}{2} + \frac{12\delta+\varsigma}{\sigma\mathcal{Q}(2/3)}\right),$$
$$\left\|\nabla_u f_{\mu=0} - \nabla_u f_{\mu(z_t)}\right\|_2 \leq \|C\|_F\|E\|_F \cdot \left(\frac{\sigma F^2\mathcal{Q}(3/4)}{2} + \frac{12\delta+\varsigma}{\sigma\mathcal{Q}(2/3)}\right).$$

□

B Interior-Point Solver and First-Order Policy Gradient Calculation

In this section, we describe the IPM solver that is used to solve the Nonlinear Complementarity Problem (NCP) in (2.4) and (2.5) (or the LCP in (3.1) that corresponds to $mu = 0$).

We adopt the primal-dual interior-point solver with Mehrotra correction (Mehrotra, 1992). Each iteration of the primal-dual interior-point solver consists a predictor step that computes the affine search direction for zero complementarity violation, and a centering (with Mehrotra correction) step that computes a target relaxation for the search direction. For notation simplicity, we consider the following form of problem:

$$\text{find } a, b, c$$
$$\text{subject to } E(a,b,c) = 0,\ b \circ c = \mu\vec{1},\ b \geq \vec{0},\ c \geq \vec{0},$$

where $a, b \in \mathbb{R}^{n\times 1}, c \in \mathbb{R}^{n\times 1}$ are the decision variables and E is the set of equality constraints. We denote $\omega := (a, b, c)$.

The solver aims to find a fixed point for the following residual:

$$\mathcal{R}(\omega;\mu) := [E(a,b,c), bc - \mu\vec{1}]^\top.$$

We denote the Jacobian of this residual with respect to the decision variables as

$$\mathcal{R}_J(\omega;\mu) := \partial\mathcal{R}(\omega;\mu)/\partial\omega,$$

where Δb_{aff} and Δc_{aff} are the corresponding elements in the affine scaling direction $\Delta_{\text{aff}} := -\mathcal{R}_J^{-1}(\omega; mu)\mathcal{R}(\omega;\mu)$.

With Mehrotra correction, we define

$$\overline{\mathcal{R}}(\omega;\mu) := [E(a,b,c), bc - \mu\vec{1} + \Delta b_{\text{aff}}\Delta c_{\text{aff}}]^\top.$$

Then the search direction Δ is given by Newton's method as

$$\Delta := -\mathcal{R}_J^{-1}(\omega;\mu)\overline{\mathcal{R}}(\omega;\mu). \tag{B.1}$$

The IPM solver adaptively relaxes the above problem by first computing the duality measure ϱ, the affine duality measure ϱ_{aff}, and the centering parameter σ:

$$\varrho := \frac{1}{n}b^\top c = \frac{1}{n}\sum_{i=1}^{n} b^{(i)}c^{(i)}, \tag{B.2}$$
$$\varrho_{\text{aff}} := \frac{1}{n}(b + \alpha_{\text{aff}}^{\text{pri}}\Delta b_{\text{aff}})^\top(c + \alpha_{\text{aff}}^{\text{dual}}\Delta c_{\text{aff}}), \tag{B.3}$$
$$\sigma := (\varrho_{\text{aff}}/\varrho)^3, \tag{B.4}$$

where $\alpha_{\text{aff}}^{\text{pri}}$ and $\alpha_{\text{aff}}^{\text{dual}}$ are the maximum step-sizes to the boundary, defined as

$$\alpha_{\text{aff}}^{\text{pri}} := \min\left(1, \min_{i:\Delta b_{\text{aff}}^{(i)}<0} -\frac{b^{(i)}}{\Delta b_{\text{aff}}^{(i)}}\right),\quad \alpha_{\text{aff}}^{\text{dual}} := \min\left(1, \min_{i:\Delta c_{\text{aff}}^{(i)}<0} -\frac{c^{(i)}}{\Delta c_{\text{aff}}^{(i)}}\right).$$

Algorithm 2 Primal-Dual Interior-Point Solver with Stopping Criteria $\texttt{SOLVER}(\mu_{\text{sc}})$

Input: Stopping criteria μ_{sc}
Initialize $a = a_0, b = b_0, c = c_0, \omega = (a, b, c)$
Update the complementarity violation $\mu_{\text{vio}} \leftarrow \max_i\{\|b^{(i)}c^{(i)}\|_\infty\}$
while $\mu_{\text{vio}} \leq \mu_{\text{sc}}$ **do**
  Calculate the duality measure ϱ, affine duality measure ϱ_{aff}, and the centering parameter σ by (B.2), (B.3), and (B.4)
  Update $\mu \leftarrow \sigma\varrho$
  Calculate the search direction Δ by (B.1), $\Delta = -\mathcal{R}_J^{-1}(\omega;\mu)\overline{\mathcal{R}}(\omega;\mu)$
  Update $\omega \leftarrow \omega + \alpha\Delta$
  Update the complementarity violation $\mu_{\text{vio}} \leftarrow \max_i\{\|b^{(i)}c^{(i)}\|_\infty\}$
end while
Output: ω

For a μ_{sc}-softened complementarity system, the predictor steps and the centering steps are performed iteratively until the complementarity violation is smaller than the stopping criteria (or tolerance threshold) μ_{sc}. Specifically, the pseudocode of the solver is provided in Algorithm 2.

In complementarity-model-based first-order policy gradient methods, the output $\omega = \texttt{SOLVER}(\mu_{\text{sc}})$ is used to replace the exact first-order policy gradient $\partial\texttt{SOLVER}(0)/\partial\theta$ by the gradient of the analytically smoothed solution $\partial\omega/\partial\theta$. In other words, for vanilla FOPG and analytically smoothed FOPG, the first-order gradient calculation in (4.2) is obtained by differentiating through the transitions governed by $\texttt{SOLVER}(0)$ and $\texttt{SOLVER}(\mu_{\text{sc}})$, respectively.

C Details of Experiments

In Section 7.1, we plot the dynamics and derivatives of the contact behavior. Here, we describe how they are generated using ordinary differential equations.

Without loss of generality, we assume that the discretization timestep size, the mass of the ball, and its initial velocity v_0 are all 1. Denote the initial vertical coordinate of the ball is q_0. Then the distance of the ball to the ground is given by $q_0 - \int\int(g - \gamma_t)\mathrm{d}t\mathrm{d}t$, where recall that γ_t is the normal impact contact force at timestep t.

Then we are able to obtain the μ-softened complementarity problem as

$$\gamma_t\Big(q_0 - \int\int(g - \gamma_t)\mathrm{d}t\,\mathrm{d}t\Big) = \mu.$$

This can be rewritten as

$$-(g - \gamma_t) = \frac{\partial^2}{\partial t^2}\frac{\mu}{\gamma_t} = \Big(-\mu\frac{\partial^2\gamma_t}{\partial t^2}\gamma_t + 2\mu\Big(\frac{\partial\gamma_t}{\partial t}\Big)^2\Big)/\gamma_t^3.$$

We simplify this second-order ODE by defining another variable e_t, such that

$$\begin{aligned}\frac{\partial\gamma_t}{\partial t} &= e_t,\\ \frac{\partial e_t}{\partial t} &= \frac{\gamma_t^4 - \gamma_t^3 g - 2\mu e_t^2}{-\mu\gamma_t}.\end{aligned} \tag{C.1}$$

Using Python to solve (C.1) gives us γ_t. Then the y-axis velocity is naturally obtained by $v_y = -\int(g - \gamma_t)\mathrm{d}t$. Since $q_x = v_0 t = t$, we get the relationship between v_y and q_x. The derivatives can be calculated using finite differences.